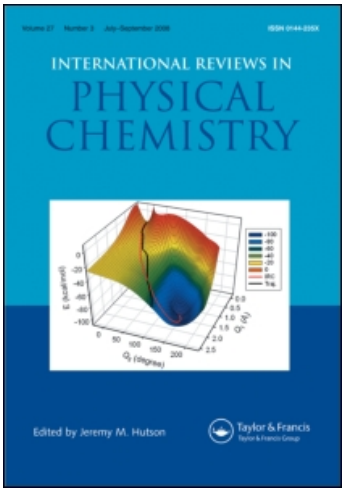

International Reviews in Physical Chemistry
Publication details, including instructions for authors and subscription information:
http://www.informaworld.com/smpp/title~content=t713724383

Spectroscopy of weakly-bound magnesium ion complexes

C. S. Yeh[a]; J. S. Pilgrim[a]; K. F. Willey[a]; D. L. Robbins[a]; M. A. Duncan[a]
[a] Department of Chemistry, University of Georgia, Athens, GA, USA

To cite this Article Yeh, C. S. , Pilgrim, J. S. , Willey, K. F. , Robbins, D. L. and Duncan, M. A.(1994) 'Spectroscopy of weakly-bound magnesium ion complexes', International Reviews in Physical Chemistry, 13: 2, 231 — 262
To link to this Article: DOI: 10.1080/01442359409353295
URL: http://dx.doi.org/10.1080/01442359409353295

INTERNATIONAL REVIEWS IN PHYSICAL CHEMISTRY, 1994, VOL. 13, NO. 2, 231–262

Spectroscopy of weakly-bound magnesium ion complexes

by C. S. YEH, J. S. PILGRIM, K. F. WILLEY, D. L. ROBBINS and M. A. DUNCAN

Department of Chemistry, University of Georgia, Athens, GA 30602, USA

Weakly bound complexes of the form Mg^+-L (L=CO_2, H_2O, N_2, Ar, etc.) are prepared in a pulsed nozzle/laser vapourization cluster source and studied in the molecular beam environment. The ion complexes are jet cooled and mass selected in a specially designed reflectron time-of-flight mass spectrometer for their study. The mass-selected ions are excited with a tunable dye laser, and the products, if any, from photodissociation are mass analysed and detected as a function of the excitation laser wavelength. This photodissociation spectroscopy experiment reveals the decomposition channels of excited complexes and their absorption spectra. Photodissociation channels vary from simple metal ion–ligand bond breaking, to metal-to-ligand charge transfer, to metal insertion/elimination reactions in the excited state. In reactive systems, the spectra are broad and featureless. However, in systems with simple metal–ligand dissociation, vibrational and partial rotational resolution is obtained in the spectra. The detailed analysis of this structure makes it possible to determine the structures of metal ion complexes and their metal–ligand binding energies.

1. Introduction

Metal containing ion–molecule complexes have been the focus of many recent experimental and theoretical studies [1–33]. These systems provide interesting models for the study of metal–ligand bonding, metal ion solvation and even metal surface–adsorbate interactions. Metal ion complexes are most easily produced and studied in mass spectrometry environments, where mass measurements provide straightforward identification of the complex species and the degree of complexation. These environments are convenient for studies of ion reaction kinetics, but the low sample densities usually preclude the study of spectroscopy. For example, several mass spectrometric studies have investigated the energetics of bonding in metal ion complexes. Equilibrium measurements in high-pressure mass spectrometers have shown the trends in binding of multiple ligands [3–5, 10]. Collision induced dissocation experiments in selected ion beams and laser photodissociation experiments in Fourier transform (FT-MS) instruments have also investigated metal–ligand dissociation energies [6–9]. Novel ion chromatography experiments have been developed to probe the interaction potential for metal ions with various gases and their state selected reactions [14]. However, there are only a limited number of spectroscopic experiments which probe the structures of metal ion complexes [15–25]. The recent progress in metal ion complex spectroscopy has been made possible by the development of laser vapourization technology for the production of higher densities of metal-containing systems and their cooling in supersonic expansions. The densities in these experiments are still too low for conventional absorption spectroscopy, but novel forms of electronic spectroscopy such as laser induced fluorescence, laser photoionization, laser photoelectron and photodissociation spectroscopy have been quite successful in molecular beam

0144–235X/94 $10·00

environments. The recent spectroscopic experiments on metal ion complexes, performed in our lab and others, have used mass-analysed photodissociation spectroscopy to select specific complexes from the distribution formed by laser vapourization cluster sources. In the present review, we describe this kind of experiment for complexes of magnesium ion with a series of small molecules and rare gas atoms.

In early photodissociation spectroscopy studies of metal ion complexes, Farrar and coworkers investigated species such as Sr^+-NH_3 and Sr^+-H_2O, including several multi-ligand complexes [15]. Brucat and coworkers have studied a variety of transition metal–rare gas dimers, as well as the ion-molecular species V^+-CO_2 and V^+-H_2O [17, 18]. The electronic spectroscopy in these complexes is characterized by metal ion atomic resonances solvated by the ligand, resulting in spectral shifts and additional multiplet structure. The work in our research group has complemented these studies and extended them to lighter metal ions where there is the possibility for interaction with theory. These studies have revealed interesting spectroscopy for metal complexes with detail not previously available, and they have uncovered fascinating photochemical dynamics. In the extension to metal ion–benzene complexes, for example, we observed the first examples of metal-to-ligand charge transfer resonances in metal complex systems [16]. We have also obtained vibrationally resolved spectra for magnesium ion with several small molecules (Mg^+-CO_2, Mg^+-N_2 and Mg^+-H_2O), which provide for the first time enough information to determine the structure of polyatomic complexes [19, 20]. Mg^+ rare gas complexes, [24] and the Mg^+-D_2 complex studied by Stwalley *et al.* [25] are some of the most weakly bound metal ion systems studied to date. Theory [26–33] and experiment agree that the bonding interactions in all of the complexes studied so far are primarily electrostatic in nature. Thus, metal ion–water complexes are bound by charge–dipole forces, metal–CO_2 complexes are bound by charge–quadrupole forces, and metal ion–rare gas systems are bound by charge-induced dipole interactions. The possible exceptions to these trends are the transition metal–molecular complexes, where open *d*-shell covalent interactions may come into play. Theory also suggests that certain magnesium ion systems will insert into their ligand upon electronic excitation [26, 30, 32, 33]. This review focuses on the research in our laboratory on magnesium ion systems, and the comparison of our experimental results with the results of recent theory on these same magnesium systems.

Magnesium ions are convenient for spectroscopy experiments for several reasons. Like the other alkaline earth cations, the ns^1 valence electron configuration results in a simple electronic spectrum dominated at low energy by an intense $^2P \leftarrow ^2S$ transition. For magnesium, this transition occurs in the ultraviolet near 280 nm [34]. Magnesium is also light enough with few enough electrons to be treated with high level *ab initio* calculations. As a result of this, Bauschlicher and coworkers have been able to carry out calculations on a variety of Mg^+-ligand complexes [26–33]. They obtain structures, vibrational frequencies and dissociation energies in both the ground electronic state and in excited states. The study of excited states produces electronic transition energies, which we have used to aid in the assignment of our spectra and to guide the search for new spectra [28–33]. Several magnesium ion complexes have now been studied in detail with both theory and experiment, and the properties obtained are in quite good agreement. Magnesium ion is also relatively unreactive with many small molecules [35]. Therefore, weakly bound complexes, rather than metal insertion reaction products, are likely to be formed when gas

phase metal ions are condensed with various gases. Finally, magnesium has three naturally occurring isotopes (24-26), which aid in the assignment and analysis of spectra with vibrational and rotational structure.

2. Experimental section

The metal ion complexes for these experiments are produced using a pulsed nozzle/laser vapourization cluster source. However, special conditions and nozzle geometries are required for the generation of cold atomic metal ions and their complexes. In particular, we use modified nozzles which enhance the production of metal atoms and decrease the tendency to form metal dimers, trimers, tetramers, etc. We also use a variety of expansion gases, and in particular seeded expansion gases, to produce the desired complexes with small molecules or rare gas atoms.

Figure 1 shows two nozzle geometrics used for these experiments, the 'cutaway' design and the 'conical' design. A normal cluster source, such as those described previously by Smalley and coworkers for the production of pure metal clusters, [36, 37] would have a small channel extending beyond the laser impact region which confines the metal vapour density and thus promotes metal–metal condensation. In some designs, a larger diameter flow region (the 'waiting room') is followed by a small constriction to increase the number of metal–metal and metal–buffer gas collisions [37]. In both the cutaway and conical source designs, however, the gas flow opens up to an expansion immediately at the laser impact zone. The metal vapour density thus drops rapidly, arresting metal–metal recombination and yielding primarily atomic metal species. In both the conventional cluster sources and those shown here, the pulsed gas undergoes a supersonic expansion with its concomitant cooling. However, the cutaway and conical nozzles minimize the channel length through which the expansion gas must flow prior to expansion and thus provide more gas density at the point of expansion. This greater density produces colder expansions than those from other source designs, which increase the efficiency of complex formation.

Metal ions are formed directly from the laser vapourization plasma in these sources. There is no downstream post-ionization. Small molecules (e.g. H_2O, CO_2, N_2) are seeded into a gas (usually argon) prior to its expansion over the metal

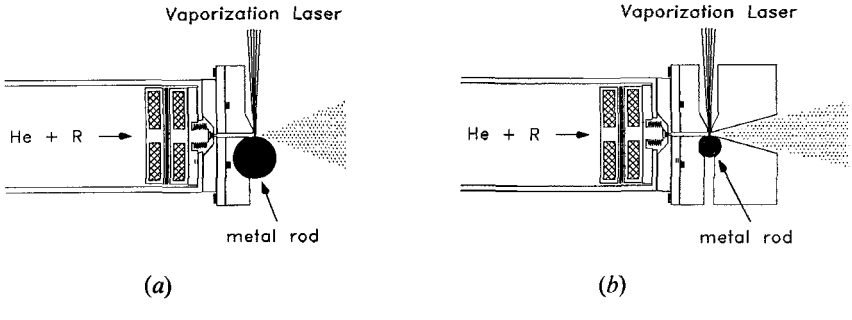

Figure 1. Cutaway (*a*) and conical (*b*) nozzle designs used in various experiments here for the production of metal ion complexes.

sample rod. The molecular species are therefore present in the hot plasma prior to expansion, but mass spectra indicate that there is very little molecular decomposition in the plasma. When the gas mixture expands just after the laser vapourization point, the small molecules or rare gas atoms condense around the metal ions, and further collisions with the expansion gas cool the complexes which are formed. The choice of nozzle design (cutaway versus conical) is determined empirically for experiments on different complexes.

The cluster sources described are part of a two chamber molecular beam apparatus as shown in figure 2. The main chamber, which contains either of the pulsed cluster sources, has a large pumping capacity (VHS-10 diffusion pump, $5000 l \cdot s^{-1}$). The second chamber contains the reflectron time-of-flight mass spectrometer system where experimental measurements are conducted. The supersonic expansions containing metal ion complexes pass from the main chamber to the mass spectrometer chamber through a skimmer which collimates the gas into a molecular beam. This beam flows through the source region of the mass spectrometer. In the mass spectrometer, pulsed acceleration plates are used to extract the ions out of the molecuar beam and turn them into the time-of-flight tube, which is mounted perpendicular to the molecular beam axis.

Three kinds of experiments are performed in the reflectron time-of-flight mass spectrometer. In the simplest experiment, the total time-of-flight of the ions through the dual tube reflectron assembly is used to measure the mass distribution of the cluster ions formed by the source. For example, figure 3 shows the mass distributions of Mg^+-Ar_x and Mg^+-$(CO_2)_x$ complexes. The argon complexes are produced in a

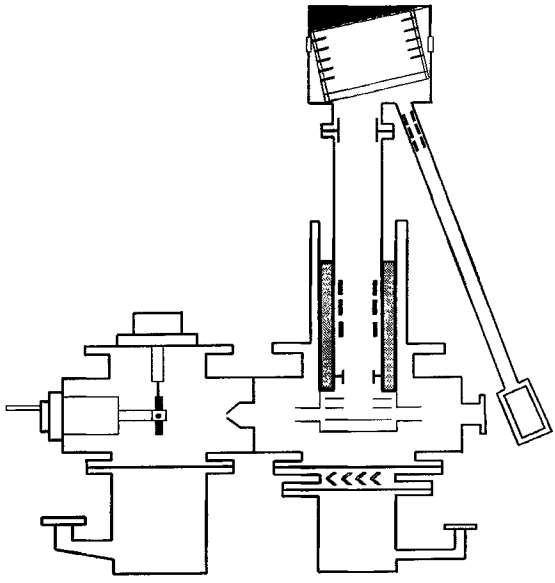

Figure 2. Two-chamber molecular beam apparatus used to study metal ion complexes. The source chamber, shown on the left, contains the pulsed valve and rotating rod metal cluster source. The expansion is skimmed before entering the second chamber, shown to the right. The reflectron time-of-flight mass spectrometer, which has two flight tube sections mounted in an inverted 'V' configuration, samples the cluster beam in the second chamber.

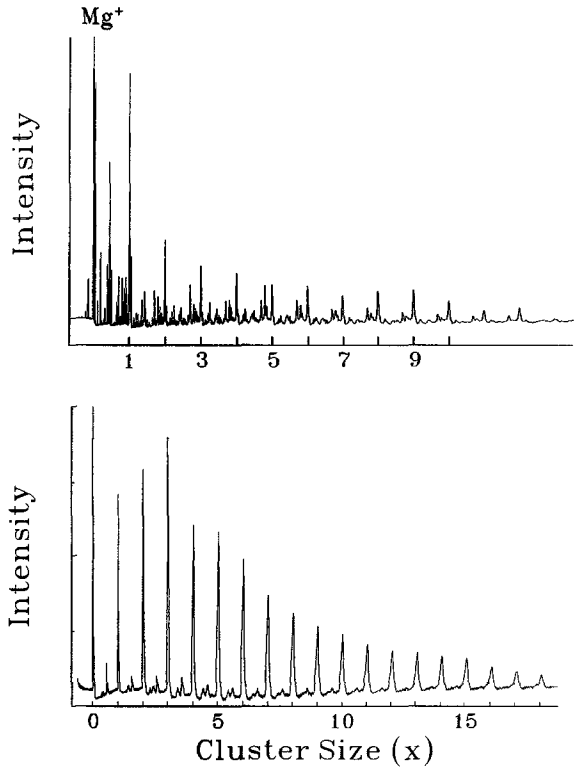

Figure 3. Mass distributions for magnesium ion–argon complexes (top) and magnesium ion–CO_2 complexes (bottom). As indicated, complexes containing multiple ligands with a single metal ion are formed efficiently up to 12 ligands for argon, and up to about 18 ligands for CO_2. The argon complex spectrum also has smaller masses corresponding to water complexes, because a small amount of added water enhances the argon clustering.

pure expansion of argon using the cutaway nozzle source, while the CO_2 complexes are produced in the conical source with a pure CO_2 expansion. For the argon complexes, a small amount of water is seeded into the expansion gas mixture to promote clustering by a mechanism which is not understood, but quite effective. This results in some water containing clusters in the mass spectrum, but these do not adversely affect the experiment because of the inherent mass analysis. Similar ion–molecule complex mass spectra are obtained for a variety of molecular and rare gas complexes with magnesium ions and with a number of other metal ions.

A second kind of experiment makes it possible to mass select any one of the ion complexes shown in these distributions and to determine their photodissociation channels at some selected laser energy. The schematic diagram of the reflectron time-of-flight mass spectrometer used for these experiments, which has been described previously, [38] is shown in figure 4. For this experiment, the mass of interest is selected by its flight time to a set of pulsed deflection plates located near the end of the first flight tube section in the reflectron. When voltages are applied to these plates, ions are deflected out of the normal trajectory through the instrument and they do not reach the detector. However, the ion of interest can be transmitted when

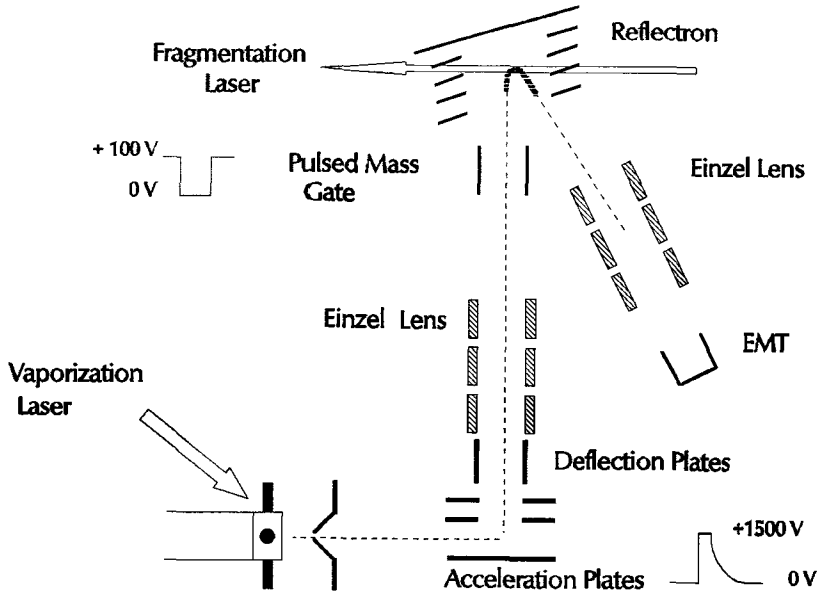

Figure 4. Reflectron time-of-flight mass spectrometer used for mass selected photodissociation experiments and photodissociation spectroscopy. Ions are selected by the pulsed deflection plates near the end of the first flight tube section and irradiated with the excitation laser in the turning region of the reflectron. The parent ions and new photofragments are mass analysed by their flight time down the second flight tube section.

a pulsed circuit switches the deflection plate to ground potential at the precise time when the desired ion passes through this 'mass gate'. The mass spectrum with the pulsed mass gate activated contains only the one mass peak selected. To study the photodissociation of this ion, a pulsed laser is introduced which crosses the ion trajectory at the turning point in the reflectron region. This laser must also be set in time to fire at the precise moment when the selected ion reaches this position in the field. The selected parent ion and any resulting photofragment ions are then accelerated together out of the reflectron field. They each attain the same energies from acceleration out of the reflecting field, but they have different velocities corresponding to their respective masses, and therefore they have different flight times from the excitation zone down the second flight tube section to the detector. The flight time through this second flight tube section therefore provides the mass analysis of the fragment ions. The resulting photofragmentation mass spectrum reveals the fragmentation dynamics of the metal complex.

An example of a photodissociation mass spectrum for the complex Mg^+–Ar is shown in figure 5. The parent ion mass selection is determined by the timing of the pulse applied to the mass gate and by the dimensions of the mass gate deflection plates. In this experiment, the mass gate resolution is able to reject all complexes except the mono-argon adduct, but the three isotopic complexes due to $^{24}Mg^+$–^{40}Ar, $^{25}Mg^+$–^{40}Ar and $^{26}Mg^+$–^{40}Ar are transmitted. However, with photoexcitation from a Nd:YAG pumped dye laser (5-ns pulse duration), it is possible to selectively excite only the $^{24}Mg^+$–^{40}Ar parent ion, which produces only the $^{24}Mg^+$ fragment ion. This kind of isotopic selectivity for photodissociation is possible

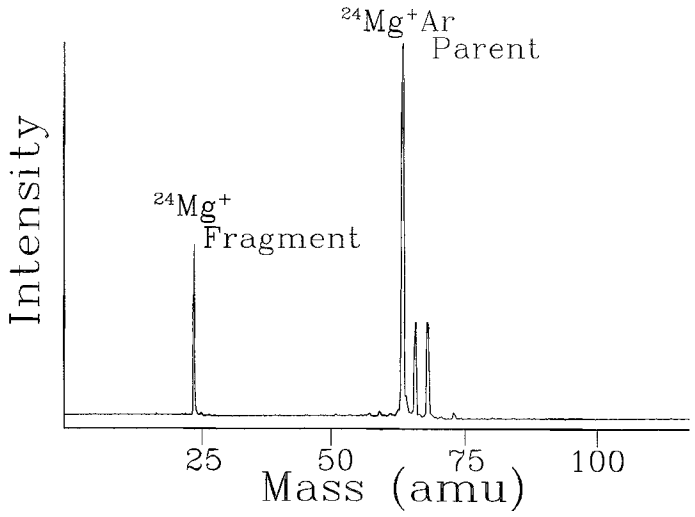

Figure 5. Photodissociation mass spectrum for Mg^+–Ar. The parent ion is shown with all three (24–26) magnesium isotopes present because the time resolution of the mass gate is not fine enough to select only one of these closely-spaced masses. However, the added time resolution provided by the pulsed fragmentation laser allows only the 24 isotope species to be excited, and therefore only the $^{24}Mg^+$ fragment ion is formed.

because of the relatively low mass of magnesium and its complexes with a variety of mono substituted ligands. This isotopic resolution is especially important in spectroscopic studies, as discussed below.

The third kind of experiment performed in the reflectron instrument is photodissociation spectroscopy, in which the wavelength (or energy) dependence of the photodissociation process is measured. In these experiments, which constitute the focus of the remainder of this chapter, the fragment ion intensity in each of the possible channels is measured while the excitation laser is tuned through a region where absorption is expected. As described earlier, magnesium ions have a strong atomic resonance line for the $^2P \leftarrow ^2S$ transition in the near UV region near 280 nm. If weakly bound metal ion complexes are formed, these complexes will contain a 'solvated' magnesium ion and their spectra will have some of the characteristics of the isolated metal ion. The absorption in the complexes is expected to be strong, but there will be shifts in energy and additional multiplet structure depending on the details of metal–ligand bonding. Photodissociation spectroscopy is based on the possibility that fragmentation of some sort will occur when these complexes are excited into these solvated metal ion resonances. As described below, such photodissociation does occur for many systems, and the resulting photodissociation excitation spectra provide an approximate measure of the absorption spectra of ion complexes. The analysis of these excitation spectra provides vibrational frequencies for the complexes and, in favourable cases, determinations of structures and dissociation energies.

3. Theoretical predictions of bonding and spectra

Theoretical studies of numerous magnesium ion complexes have been reported by Bauschlicher and coworkers [26–33]. These studies have determined the structures, dissociation energies and spectra for these complexes. Theory supports the

general notion that the magnesium ion is not very reactive in its ground electronic state [26]. Therefore, when Mg^+ binds to small molecular species, the interaction is primarily electrostatic in nature. This means that magnesium systems can properly be regarded as ion–molecule complexes, and that simple electrostatic concepts can be used to conceptualize the resulting bonding. Thus, *ab initio* theory and simple electrostatics are both useful in describing the bonding and spectra to be expected for these complexes. Of particular interest for our research, these considerations indicate that the ligand binding in both the ground and excited electronic states of the complex can be used to determine the characteristics of the electronic absorption spectrum. The relative binding energies in the two states determine the shift in the complex spectrum relative to the atomic resonance line, and the possible orientations of the ground *s* orbital or excited *p* orbital on Mg^+ relative to the ligand determines how many electronic states will correlate to the atomic resonance. For example, figure 6 shows the pattern of energy levels and states expected for any linear Mg^+–ligand complexes. This pattern would apply for Mg^+–rare gas complexes, with charge-induced dipole binding interactions, and for complexes with linear ligands if they are bound so that the overall complex is also linear. For example, linear molecular complexes are predicted by Bauschlicher and coworkers for Mg^+–CO_2 and Mg^+–N_2 [28, 33]. Simple electrostatics would also make the same prediction for these systems. Although neither molecule has a permanent dipole moment, they both have negative quadrupole moments [40]. The charge–quadrupole interaction is therefore favoured in the linear configuration.

A $^2\Sigma^+$ ground state is expected for these various linear systems, correlating to the Mg^+ (^2S)+*L* (^1S or $^1\Sigma$) asymptote. Two molecular excited states, $^2\Pi$ and $^2\Sigma^+$, correlate to the atomic Mg^+ (^2P)+*L* (^1S or $^1\Sigma$) asymptote. These correspond,

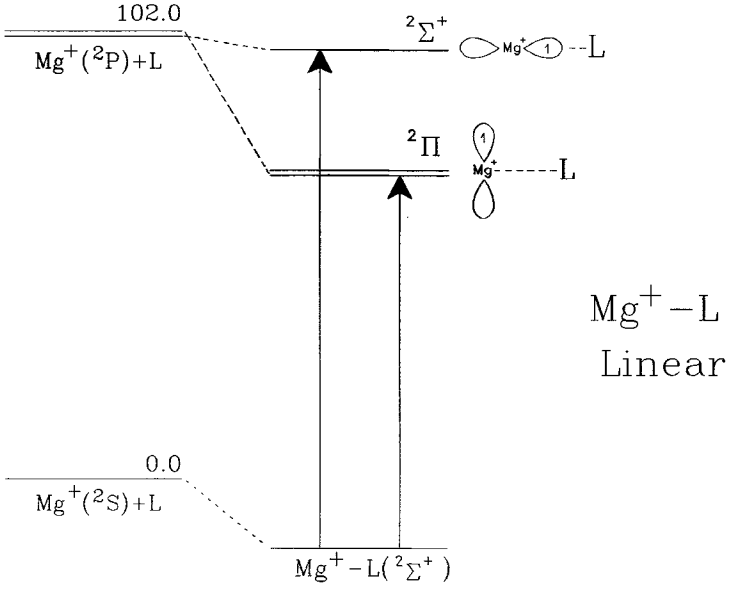

Figure 6. Energy level diagram for linear Mg^+–*L* complexes such as Mg^+–Ar, Mg^+–CO_2 or Mg^+–N_2.

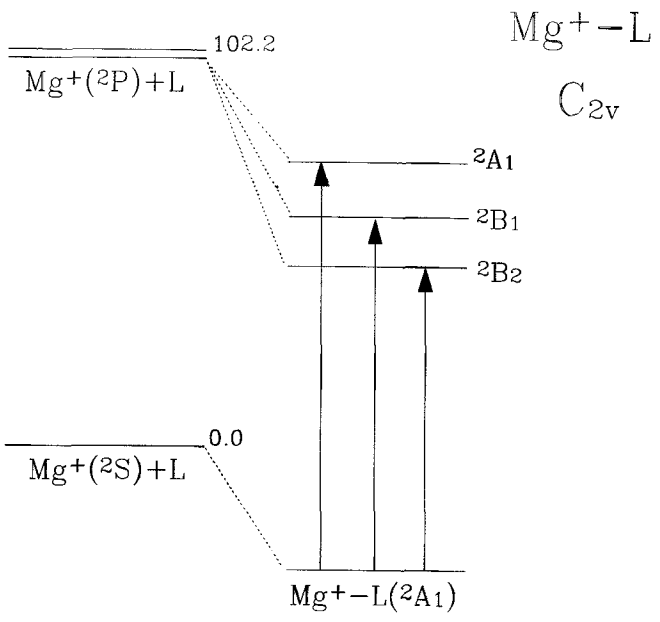

Figure 7. Energy level diagram for Mg^+–L complexes with C_{2v} symmetry, such as Mg^+–H_2O.

respectively, to the perpendicular and parallel orientations of the excited Mg^+ *p* orbital with respect to the molecular axis. Electronic transitions from the ground state to either excited state are allowed, and should be observable in the spectroscopy. The electrostatic interaction in the excited $^2\Pi$ state is expected to be relatively strong because the *p* orbital orientation exposes the doubly positive core of Mg^+ to the ligand. However, the electrostatic binding in the ground and excited $^2\Sigma^+$ states are expected to be relatively weak, because of on-axis electron density which shields against this interaction. The shielding is greater in the excited state, with the on-axis *p* orbital. Therefore, we expect the $^2\Pi$ state to be more strongly bound than the ground state, resulting in a $^2\Pi \leftarrow ^2\Sigma^+$ transition red shifted from the atomic resonance line. The excited $^2\Sigma^+$ state will be more weakly bound than the ground state and the $^2\Sigma^+ \leftarrow ^2\Sigma^+$ transition should be blue shifted from the atomic resonance. The vibrational structure in the $^2\Pi \leftarrow \Sigma^+$ transition should be doubled by the $^2\Pi_{1/2,\,3/2}$ spin–orbit splitting. These general predictions are born out, as discussed below, in several linear complex systems.

Nonlinear molecular ligands necessarily result in other symmetry species when they form metal ion complexes. The specific symmetry found depends on the exact details of the bonding. However, another common complex symmetry for small molecular ligands is C_{2v}. C_{2v} complexes are expected for Mg^+–H_2, Mg^+–C_2H_2 and Mg^+–C_2H_4, all of which have ligands with no dipole moments [30, 33]. However, the positive quadrupole moments of these species result in side-on charge–quadrupole interactions. Another system expected to have C_{2v} symmetry is Mg^+–H_2O, whose binding is charge–dipole [26, 29]. The energy level pattern for a C_{2v} complex is shown in fig. 7. A single ground state level of $^2A_1$ symmetry correlates to

the Mg^+ (^2S)+L asymptote. However, there are now three excited electronic states which correlate to the Mg^+ (^2P)+L asymptote. These three states correspond to the metal ion–ligand orientations which have the excited p orbital on the C_2 axis ($^2A_1$), perpendicular to it and in the plane of the molecule ($^2B_2$) and perpendicular/out-of-plane ($^2B_1$). As found in the linear complexes, the energy ordering of these excited states depends on the details of the bonding. The states which have the doubly positive Mg^{2+} core exposed to the ligand (B_1 and B_2) have greater electrostatic interactions than the on-axis orbital configuration in the A_1 state where there is greater shielding by the valence electron. The specific configuration of the orbitals in the two perpendicular configurations must also be considered. Figure 7 shows the order which results for the Mg^+–H_2O complex, where the p orbital interactions with the oxygen lone pairs make the in-plane configuration on the $^2B_2$ state more stable [29]. These two states are reversed in energy, with B_1 lower than B_2, for the Mg^+–acetylene and Mg^+–ethylene complexes [33].

In the same way discussed earlier, the binding details in these ground and excited states can be combined to obtain an overall picture of the electronic spectra to be expected. Transitions are allowed from the ground $^2A_1$ state to each of the three excited states in C_{2v} symmetry. The enhanced binding in the excited states result in $^2B_1 \leftarrow {}^2A_1$ and $^2B_2 \leftarrow {}^2A_1$ transitions which are red shifted with respect to the atomic resonance line, while the $^2A_1 \leftarrow {}^2A_1$ transition is expected to be blue shifted with respect to the atomic line. The exact positions of the $^2B_1 \leftarrow {}^2A_1$ and $^2B_2 \leftarrow {}^2A_1$ transitions depend on which of the excited states is more strongly bound.

While many of the magnesium ion complexes under investigation here remain electrostatically bound in both their ground and excited states, some exhibit more complex interactions. For example, theory predicts that magnesium ion and oxygen form an ion pair complex of the form Mg^{2+}, O_2^- in the complex ground state [31]. Other species have simple electrostatic interactions in the ground electronic state, but undergo reaction in the excited state. In these systems, a common scenario is that the metal ion reaction with the ligand is endothermic in the ground electronic state, but when the metal ion is excited electronically a reaction becomes energetically possible. Theory predicts excited state reactions for the complexes Mg^+–H_2, [30] Mg^+–N_2, Mg^+–acetylene and Mg^+–ethylene [33]. Mg^+–CH_4 is predicted to bind electrostatically in a 2-H bridged position in the ground state, but in a 3-H site in the excited state [32]. Each of these various interactions provides richness to the metal ion chemistry, but they introduce severe complications for spectroscopy. Stwalley and coworkers have observed the MgD^+ channel in the photodissociation spectra of Mg^+–D_2, consistent with the predicted excited state reaction [25]. Misaizu *et al.* have reported reactive channels in the dissociation spectra of Mg^+–H_2O [23]. Our results described here provide the only other investigations of these phenomena.

4. Magnesium ion–rare gas complexes

Figure 8 shows the photodissociation excitation spectra for the simplest weakly bound magnesium ion complexes, Mg^+–Ar, Mg^+–Kr and Mg^+–Xe. In each of these spectra, the parent ion complex is mass selected and the appearance of the Mg^+ fragment ion is measured as the excitation laser is scanned. Because of the parent and fragment mass analysis in the experiment, these spectra can be unequivocally assigned as electronic excitation spectra for the indicated metal ion–rare gas (RG) dimers. However, it is important to consider the mechanism which gives rise to these spectra before investigating their specific assignments. The best interpretation of

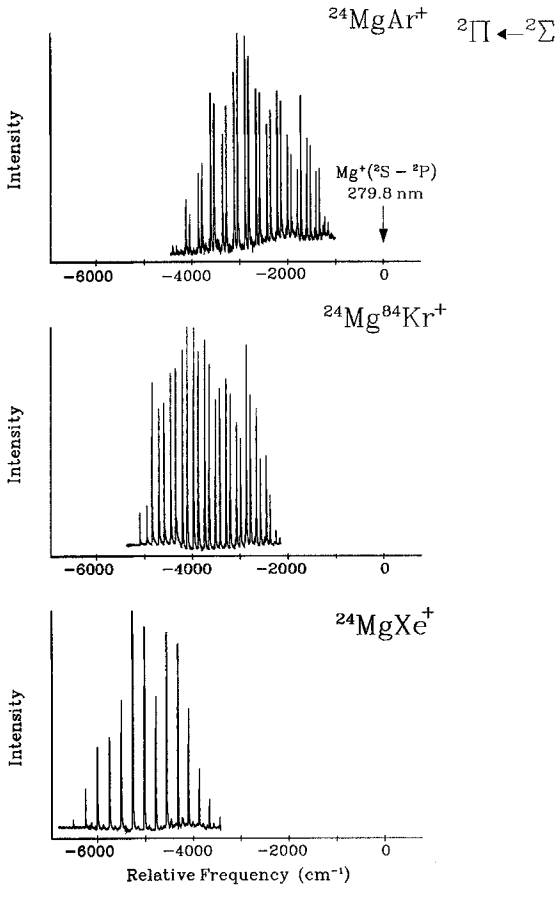

Figure 8. Photodissociation spectra of Mg^+–Ar, Mg^+–Kr and Mg^+–XE. All three spectra are plotted on the same scale so that their special positions can be compared with each other and to the position of the atomic resonace line.

these spectra is that they result from resonance enhanced multi-photon dissociation (REPD) [19, 20]. This interpretation is the only one consistent with the overall large cross-sections for the photodissociation processes (10^{-17} to 10^{-18} cm^2) and the sharp vibrational features observed. Only a single-photon resonant process could produce the large signals observed. Predissociation at the one-photon level can be ruled out because non-radiative decay efficient enough to produce such large signals would also likely result in significant line-broadening. Resonant absorption to sharp bound states at the one photon level followed by dissociation at the second (or higher) photon level is consistent with all the known facts for these complex spectra and the others described later. Since these spectra result from resonances at the one photon level, they are essentially equivalent to absorption spectra in their line *positions*. The caveat in this picture is that the line *intensities* may be affected by other resonances in the second or higher photons. However, while we do measure different overall cross-sections for photodissociation of different complexes, the spectra we measure for any given complex vary smoothly in intensity over the

regions studied. It therefore seems that this latter possible complication has not yet been realized.

All three photodissociation spectra shown here have a series of sharp lines beginning to the red of the atomic transition and extending for about 3000 cm^{-1}. The red shift is greatest for the xenon complex and smallest for the argon complex. In each spectrum, there is a series of sharp lines, but the patterns in these lines is not the same for the three complexes. The argon spectrum appears to have a series of doublets with a close spacing of about 75 cm^{-1}, and these doublets are spaced about 250 cm^{-1} from each other. The krypton spectrum has nearly equally spaced lines and the xenon spectrum also has a series of very closely spaced doublets. Based on the discussion above, we expect that electronic spectra to the red of the atomic resonance line should be associated with the $^2\Pi_{1/2,\,3/2} \leftarrow {}^2\Sigma^+$ transition for each rare gas. We therefore expect to see structure from vibrational progressions as well as structure associated with the $^2\Pi_{1/2,\,3/2}$ spin–orbit splitting. To unravel the various possibilities, we study isotopic variations for these spectra, and we consider the likely magnitude to be expected for spin–orbit splittings.

The spin–orbit splitting in the Mg^+ ($^2P_{1/2,\,3/2}$) atomic state is 91·55 cm^{-1}. This value corresponds to 3/2 A in the Hund's case (c) coupling scheme appropriate for the magnesium ion [39]. However, in the molecular complex, the appropriate coupling scheme is Hund's case (a), in which the observed splitting in the $^2\Pi_{1/2,\,3/2}$ state should be exactly A, or 61·0 cm^{-1} [39]. There are no splittings in any of the magnesium ion rare gas complex spectra which are 61 cm^{-1}, but the multiplet in the argon complex spectrum is about 75 cm^{-1}. We therefore suspect that this is the spin–orbit splitting in this complex, but we also perform isotopic measurements to confirm this.

Isotopic measurements are important because the three isotopomers of each complex (i.e. $^{24}Mg^+$–Ar, $^{25}Mg^+$–Ar and $^{26}Mg^+$–Ar) will have slightly different vibrational frequencies in both the ground electronic state and the excited electronic state involved in these spectra. Because of these slightly different frequencies, vibronic bands with the same vibrational quantum numbers will appear shifted when the spectra for different isotopomers are measured. These shifts should have essentially the same values in both of the components of the $^2\Pi_{1/2,\,3/2}$ state. Therefore, the shifts of the different lines can be used to identify which doublets arise from spin–orbit effects and which lines are caused by the vibrational progressions. For argon, each of the pairs of lines with the spacings near 75 cm^{-1} have the same isotopic shifts. Therefore, the 250 cm^{-1} spacings represent the vibrational progressions and the 75 cm^{-1} spacings are the spin–orbit multiplets. In the krypton complex spectrum, the first two lines at low energy have the same isotopic shift, as do each subsequent pair. This means that the spin–orbit spacing is about 140 cm^{-1}, and the vibrational spacings are about 250 cm^{-1}. For the xenon complex, the first two lines again have the same isotopic shift. The closely spaced 12–13 cm^{-1} doublets, which are only visible when the spectrum in figure 8 is expanded slightly, arise from the close proximity of v ($^2\Pi_{3/2}$) and $v+1$ ($^2\Pi_{1/2}$) lines. The vibrational spacings are again about 250 cm^{-1}, while the spin–orbit splittings are about 260 cm^{-1}. The vibrational spacings in these three spectra are therefore all very similar, while the spin–orbit splittings increase dramatically for the series Ar, Kr, Xe.

In each of the three spectra shown, there is a gradual decrease in the spacings attributed to vibrational bands as one proceeds toward higher energy. This observation, and the expectation that the supersonic beam produces cold complexes, leads

to the conclusion that the intense lines observed here in each spectrum are excited state progressions originating from the ground vibrational state (i.e., $v''=0$). However, there are also weak satellite bands in each spectrum which can be assigned as vibrational hot-bands originating from $v''=1$. These bands appear to the red of several of the intense bands, providing multiple determinations of the respective ground state fundamental frequency, $\Delta G_{1/2}''$. The values determined are 96, 112 and 120 cm^{-1} for the argon, krypton and xenon complexes.

Having determined that the lower state in the intense progressions is $v''=0$, we must assign the excited state vibrational levels. However, in electronic transitions such as these where extensive vibrational progressions are measured, special care must be taken to assign the vibrational quantum numbers. The origin of the electronic transition may have weak Franck–Condon intensity or be absent from the spectrum if there is a large geometry change between the two states involved in the transition, and it is just such a geometry change which causes long progressions like those observed here. Again, isotopic shifts in the spectrum provide the way to determine which band is the origin and therefore the exact quantum numbering for all the bands.

The isotope shift expected for an electronic transition of a diatomic molecule is: [41]

$$\Delta G_{iso}(v', v'') = (1-\rho)[\omega_e'(v'+1/2) - \omega_e''(v''+1/2)] - (1-\rho)^2[\omega_e x_e'(v'+1/2)^2 - \omega_e x_e''(v+1/2)^2],$$

where ΔG_{iso} is the shift for a particular vibrational band with initial and final vibrational levels indicated, ω_e and $\omega_e x_e$ are standard vibrational constants for the ground and excited states, and ρ is the reduced mass ratio, $\rho=(\mu/\mu_{iso})^{1/2}$. Therefore, if we knew the Mg^+–*RG* stretching vibrational constants in the ground and excited states, it would be possible to calculate the isotope shift. However, we cannot determine the vibrational constants until we assign the quantum numbers. Additionally, we have no measurements on the ground electronic state. To circumvent this problem, we use trial assignments of the vibrational numbering in the excited state, which produces values for ω_e' and $\omega_e x_e'$. We then use estimated parameters for the ground state vibrational constants. As described above, we observe hot-bands resulting in the determination of the ground state fundamental frequency ($\Delta G_{1/2}''$) for Mg^+–Ar, Mg^+–Kr and Mg^+–Xe of 96, 112 and 120 cm^{-1} respectively. We use these values of $\Delta G_{1/2}''$ in place of ω_e'' in the above equation, and we neglect the anharmonicity. This procedure introduces some errors, but since the only quantum number involved in the ground state is the $v=0$ vibrational level, the influence of these approximations on the overall determination is small. We finally calculate the isotope shift expected for each of several trial assignments of the excited state quantum numbers. A comparison of the calculated and measured shifts determines the best vibrational assignment.

A typical isotopic shift experiment is shown in figure 9 for Mg^+–Ar. The lines indicate the isotope shifts calculated using different assumptions for the vibrational quantum numbering of the first band in the spectrum. The solid circles are the measured shift between corresponding bands in the $^{24}Mg^+$–Ar and $^{25}Mg^+$–Ar spectra. As shown, the measured shifts are in best agreement with the shifts expected if the first band in the spectrum results from the $v'=0 \leftarrow v''=0$ transition. Therefore, the origin band is found to be the first band in this system, and the subsequent bands

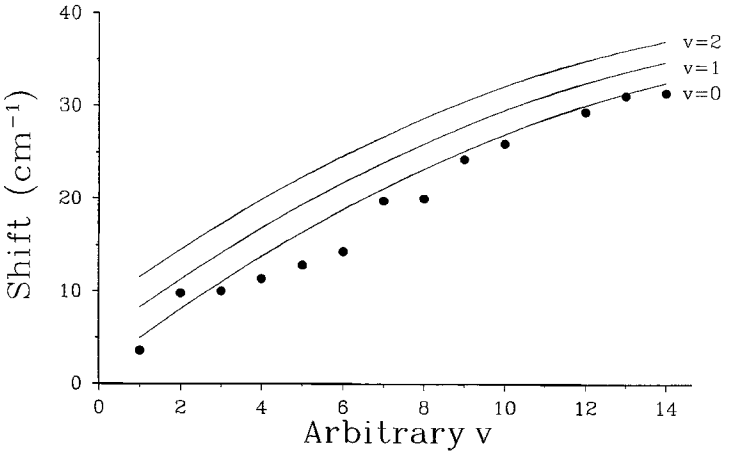

Figure 9. Isotope shift experiment for $^{24}Mg^+$–Ar against $^{25}Mg^+$–Ar, used to determine the exact quantum number assignments for the vibrational levels. The shifts predicted (—) with the first level in the upper state assigned to anything other than the $v=0$ level are too large for the observed shifts (●).

can be assigned to higher quantum number transitions. This same kind of analysis leads to the conclusion that the first line observed in the Mg^+–Kr spectrum is the $v'=1 \leftarrow v''=0$ band, and that the first band observed for the Mg^+–Xe complex is the $v'=2 \leftarrow v=0$ transition.

Having determined the quantum number assignments for the various bands in the three spectra, we apply the standard form equation to determine the vibrational constants: $\Delta G(v')=\omega_e'(v'+1/2)-\omega_e x_e'(v'+1/2)^2$. A least squares fit of the observed vibrational band positions to this equation produces the vibrational constants shown in table 1. As indicated, we have calculated the constants for both components of the spin–orbit doublets. Additionally, we have used the vibrational constants determined from our fit to extrapolate to the positions of the missing origin bands in the Mg^+–Kr and Mg^+–Xe spectra, which are given in parentheses in table 1.

As shown in table 1, the excited vibrational frequency for Mg^+–Ar is the largest of the three (272 cm^{-1}), while the Mg^+–Kr and Mg^+–Xe complexes both have

Table 1. Spectroscopic constants for $^{24}Mg^+$-rare gas complexes [24]. The origin positions shown in parentheses are not observed directly, but are determined by extrapolation with the vibrational constants. All entries are in cm^{-1}.

	$^2\Pi_{1/2}$			$^2\Pi_{3/2}$			$X^2\Sigma^+$
RG	ν_{00}	ω_e	$\omega_e x_e$	ν_{00}	ω_e	$\omega_e x_e$	$\Delta G_{1/2}$
Ar	31 396	271·8	3·25	31 472	271·9	3·29	96
Kr	(30 464)	257·7	2·29	(30 608)	255·5	2·26	112
Xe	(28 825)	258·0	1·49	(29 093)	254·6	1·50	120

Table 2. Ground and excited state dissociation energies for Mg^+–*RG* and Na–*RG* [24]. The Mg^+–*RG* data are determined by a Morse potential extrapolation, followed by the cycle: $D_0'' = \nu_{00} + D_0' - [^2P_{1/2} \leftarrow {}^2S_{1/2}]$. All units are in cm^{-1}.

	Mg^+–*RG*		*Na–RG*	
RG	$X^2\Sigma^+$	$A^2\Pi_{1/2}$	$X^2\Sigma^+$	$A^2\Pi_{1/2}$
Ar	1189	5554	40	568
Kr	1831	7128	69	790
Xe	4090	11 026	117	1215

the slightly lower value of $258\,cm^{-1}$. These frequencies are influenced by both the masses of the species present and the force constant of the complex bond. Since the bonding is electrostatic in nature, the strength of the bonding, and therefore the vibrational force constant, should increase for the more polarizable rare gases krypton and xenon. This effect would tend to increase the vibrational frequency for the series Ar, Kr, Xe. However, the reduced mass of the complexes increases for the heavier rare gases, which tends to reduce the frequencies for the series Ar, Kr, Xe. These competing effects produce the overall vibrational frequency trend. Apparently, the mass effect outweighs the importance of the binding strength in the case of the argon complex, while the two factors offset each other almost exactly for krypton and xenon. In the ground state, the trend seems to be somewhat reversed, with the heavier complexes having higher frequencies. Interestingly, the ground state frequency for Mg^+–Ar ($\Delta G_{1/2} = 96\,cm^{-1}$) is in good agreement with the value calculated by Bauschlicher and coworkers ($\omega_e = 98\,cm^{-1}$) [27]. It is also close to, but slightly higher than the value we have measured with high-resolution photoelectron spectroscopy for the ground state of Al^+–Ar ($\omega_e'' = 67\,cm^{-1}$) [22].

The long vibrational progressions measured here for each of these complexes make it possible to determine their dissociation energies in both the ground and excited electronic states. The excited state values are determined by the extrapolation of the vibrational spacings to the point where they converge, and by the assumption of some mathematical form for the potential. Precise mathematical forms for the potential in electrostatic systems have been described by LeRoy and Bernstein [42]. However, as we have discussed elsewhere, [19, 20, 24] the LeRoy–Bernstein formalism produces anomalous results unless levels at or near the dissociation limit are measured. In the rare gas systems here we measure extensive progressions, but the levels measured cover no more than about the lower half of the potential. We have found the best agreement with high level *ab initio* calculations and other experiments when we use the simpler and more familiar treatment for dissociation energies described by Birge and Sponer [41]. The Birge–Sponer plot, in which the spacings between successive vibrational levels $\Delta G_{v+1/2}$ are plotted against the vibrational quantum number $v + 1/2$, inherently assumes that a Morse potential is appropriate for the system. The dissociation limit is then related to the Morse vibrational constants already determined above, $D_e = \omega^2/4\omega_e x_e$. Subtraction of the zero point energy produces D_0, i.e. $D_0 = D_e - \omega_e/2 + \omega_e x_e/4$. However, this treatment for the spectra described here produces dissociation energies in the excited $^2\Pi$ state. The values obtained which are shown in table 2, are 5554, 7128 and $11\,026\,cm^{-1}$ for the argon, krypton and xenon complexes respectively. The ground state dissociation

energy is the more interesting value, and this can also be derived from the data available here, as shown in figure 10. The extrapolation of the vibrational levels eventually reaches the atomic Mg^+ ($^2P_{1/2}$)+RG (^1S) asymptote. This level lies above the ground state Mg^+ (^2S)+RG (^1S) asymptote at an energy given by the atomic transition (35 669 cm^{-1}). As described earlier, we have measured the energy of the origin bands in each of the complexes. Therefore, the ground state dissociation energies can be determined from the simple cycle,

$$D_0'' = \nu_{00} + D_0' - (^2P_{1/2} \leftarrow {}^2S_{1/2}).$$

The ground state dissociation energies for the three magnesium ion–rare complexes are shown in table 2. Also shown in table 2 are the dissociation energies determined previously for the series of isoelectronic Na–rare gas van der Waals complexes. The Mg^+–RG dissociation energies are much greater than the Na–RG values, as expected because of the greater strength of charge induced dipole forces compared to van der Waals forces. However, it is interesting that the trend in values for the two series are similar. In both series, the excited $^2\Pi$ state dissociation energies are much greater than the ground state values. The difference is about an order of magnitude in the neutral Na systems, while it is a factor of 3–5 in the ion systems. In both series, the binding energies are greater for the heavier rare gases. This is expected because the larger rare gases are more polarizable, and the charge-induced dipole

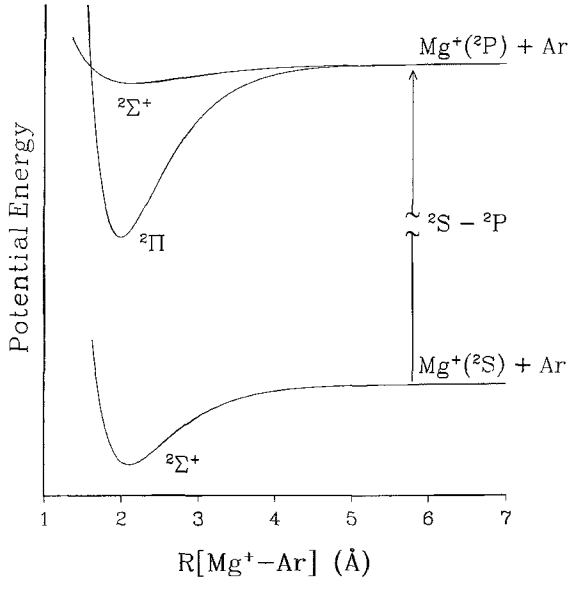

Figure 10. Schematic energy level diagram for the Mg^+–Ar complex showing the approximate well depths in the various states and their asymptotes. The observed electronic origin in the complex, the well depth in the excited state, and the known asymptotic energy for the atomic transition can be combined to determine the ground state well depth.

interaction scales with the polarizability. However, this trend is not quantiatively followed, as discussed in our previous work [24]. The xenon systems are more strongly bound than would be expected by their greater polarizability alone.

A final interesting aspect of these rare gas complex spectra is their spin–orbit interaction. As mentioned above, the spin–orbit splitting in these complexes should be equal to the value of 61 cm^{-1}. However, the actual value is greater than this for each of the rare gas complexes studied. It is about 75, 140 and 260 cm^{-1} for the argon, krypton and xenon complexes, respectively. Moreover, the values measured for these systems vary with the vibrational state. Due to space considerations, we do not present the tabulated line positions here, and the small variations in the splitting observed are not evident in the spectra shown in figure 8. Nevertheless, there is a clear pattern of decreasing spin–orbit splittings observed for all three complexes as the vibrational quantum number increases, which is documented in our original paper on these complexes [24]. The variation in the spin–orbit splitting with the vibrational level is approximately linear. Similar observations have been described previously for the isoelectronic Na–*RG* systems [43–47]. The large spin–orbit splitting and the vibrational state dependence have two possible explanations, which have been discussed in detail by Breckenridge [43]. Both are caused by the mixing of the normal spin–orbit interaction of the metal ion with the spin–orbit interaction of rare gas atom states. In one possible scenario, a small admixture of excited rare gas character results from distortion of the rare gas electron distribution by the metal ion. For example, in excited Rydberg states of the form $np^5(n+1)s^1$, the rare gas wavefunction has a '*p*-hole' character and these states have large spin–orbit splittings. The spin–orbit splittings in these excited states are essentially the same as those in the respective rare gas ions, as indicated in table 3. These rare gas Rydberg states have the correct symmetry to mix into the wavefunction of the $Mg^+(p\pi)$–*RG* states, and, since the rare gas splittings are so large, only a small admixture is enough to explain the difference between the complex values and that of isolated Mg^+. The increasing trend in the argon, krypton and xenon complexes is consistent with the trend in splittings for these three rare gas atoms. Additionally, the greater polarizability down this series would favour more extensive distortion of the heavier rare gas atoms. The vibrational dependence of the interaction is explained by the closer approach of the rare gas atom to the metal ion in lower vibrational states, which enhances the interaction. As discussed by Breckenridge, if this mixing mechanism is active, the spin–orbit states become inverted with the $\Pi_{3/2}$ level lying lower than the $\Pi_{1/2}$ level [43]. Without rotational resolution, we cannot identify the

Table 3. $^{24}Mg^+$–rare gas complex spin–orbit coupling constants, and the comparison to the value for the isolated Mg^+ atomic ion and the respective spin–orbit splitting (S.O.S) values for excited rare gas atoms and ions [24]. All units are cm^{-1}.

Complex	A_e*	α_A*	S.O.S.$_{RG}[np^5(n+1)s^1]$	S.O.S.$_{RG\ ion}[np^5]$
Mg^+–Ar	77·0	0·47	1 649	1 431
Mg^+–Kr	143·0	1·77	5 220	5 371
Mg^+–Xe	270·4	3·49	9 129	10 537
Mg^+	61·0			

* Determined from a linear extrapolation of $A(v)=A_e-\alpha_A(v+1/2)$.

spin–orbit levels. However, the vibrational dependence of inverted levels would be manifested as a decreasing negative splitting for higher vibrational states, eventually passing through zero, and then an increasing positive splitting for non-inverted levels which would be approximately the atomic value at the dissociation limit of the complex. In our systems, the vibrational state dependencies of the spin–orbit splitting for the complexes are linear, and if they are extrapolated there is a smooth dependence toward the isolated metal ion spin–orbit value at approximatley the dissociation energy of the complex [24]. Therefore, there is no apparent evidence for inverted levels, but the long extrapolations involved here cannot be taken to provide a definitive test of this effect. Another mechanism suggested by Breckenridge preserves the normal order for the spin–orbit levels. The excited p orbital in the $^2\Pi$ state exposes the rare gas atoms to the doubly positive Mg^{+2} core of Mg^+, and if the excited p electron density is diffuse enough, configurations of the form Mg^{2+}–$RG(np^6p\pi)^-$ could be mixed into the wavefunction of the excited states. The spin–orbit splittings for the relevant rare gas negative ion states are not known, but they should be large like the p-holes states. Although this mechanism may seem unconventional, it could explain the large spin–orbit splitting observed with a regular $^2\Pi_{1/2,\,3/2}$ level ordering. Future rotationally resolved spectra on these systems will be able to determine the true level order observed and address these interesting questions about the spin–orbit interaction in these systems.

Although there have been previous studies of metal ion–rare gas complexes, [17] the series of Mg^+ complexes described here provides the only set with which to investigate the trends for the different rare gases. The binding energies of the magnesium ion complexes are significantly less than those observed for transition metal ions [17]. Additionally, the spin–orbit effects described here have not been documented previously for other metal ion systems. Through the interaction with theory, this data could provide a quantitative measure of the degree of charge delocalization in these systems. While theory has been applied to the excited states of some of the other magnesium ion complexes, it has not been used for the rare gas systems. We anticipate the availability of such theory in the future. We also are in the process of setting up new experiments with higher resolution which will provide rotationally resolved spectra for these systems.

5. Mg^+–CO_2 complexes

Magnesium ion complexes with carbon dioxide are produced in a pure expansion of CO_2 using the conical nozzle source [19]. Complexes containing up to 18 CO_2 molecules have been studied with fixed energy photodissociation [48]. The average evaporation energy per molecule is found to be significantly greater than the value for bulk solid CO_2, and this average energy per molecule decreases smoothly as the complex size increases. The spectroscopy of these systems was facilitated by *ab intitio* calculations by Bauschlicher and coworkers, which guided our initial search for excitation spectra for Mg^+–CO_2 and Mg^+–$(CO_2)_2$ complexes [28]. These calculations find that Mg^+–CO_2 is linear, and that it is bound by the charge–quadrupole interaction. The ground state binding energy is predicted to be 16·4 kcal mol^{-1}, and the Mg^+–O bond distance in the ground state is predicted to be 2·10 Å. The electronic states and energy pattern for this complex are therefore qualitatively the same as those for the rare gas complexes. The spectrum is expected to consist of a $^2\Pi \leftarrow {}^2\Sigma^+$ transition red shifted from the atomic transition. Theory predicts that the red-shift for this complex should be about 5000 cm^{-1} [28].

The excitation spectrum measured for Mg^+–CO_2 is shown in figure 11. It consists of a series of six doublets, with the first member of the series occurring at 29 625 cm^{-1}. The doublets in the spectrum are spaced by 56 cm^{-1}, and the larger spacings in the spectrum are about 380 cm^{-1}. The spectrum is observed in the Mg^+ fragment ion channel. A second region of continuous absorption (not shown here), in which both the Mg^+ and MgO^+ fragment ions are observed, occurs near 266 nm and is assigned to the $^2\Sigma^+ \leftarrow ^2\Sigma^+$ transition [49]. This spectrum is analysed using the same procedures and methods discussed above for the rare gas complexes.

By analogy to the rare gas complex spectra, and because theory predicts the complex to be linear, we expect that the 56 cm^{-1} doublets arise from the $^2\Pi_{1/2,\,3/2}$ spin–orbit splitting. Isotopic studies like those described above confirm this. The doublet spacing is invariant upon substitution of the magnesium isotopes, but the larger spacings in the spectrum are reduced for the heavier complexes. The observation of this spin–orbit multiplet structure also confirms that the complex is linear. The isotope shifts of the various bands also establish that the first peak in the spectrum is the origin band of the system [19]. The series of strong doublet bands are assigned to a single progression of the form $v'=0, 1, 2, 3, 4, 5 \leftarrow v''=0$, with a frequency of $\omega'_e = 381{\cdot}8\ cm^{-1}$ and an anharmonicity of $\omega_e x'_e = 3{\cdot}20\ cm^{-1}$ ($^{24}Mg^+$–CO_2). The weakly bound complex suggested by theory should have much higher frequencies corresponding to the internal modes of the CO_2 molecule. Low frequencies such as this are only expected for the metal stretching and bending modes. For a linear complex, the bending modes are vibronically forbidden, but the stretching mode is vibronically allowed. The Franck–Condon factors for the transition also are expected to be favourable for the stretching mode, because theory predicts a significant contraction of the metal–ligand bond distance in the excited

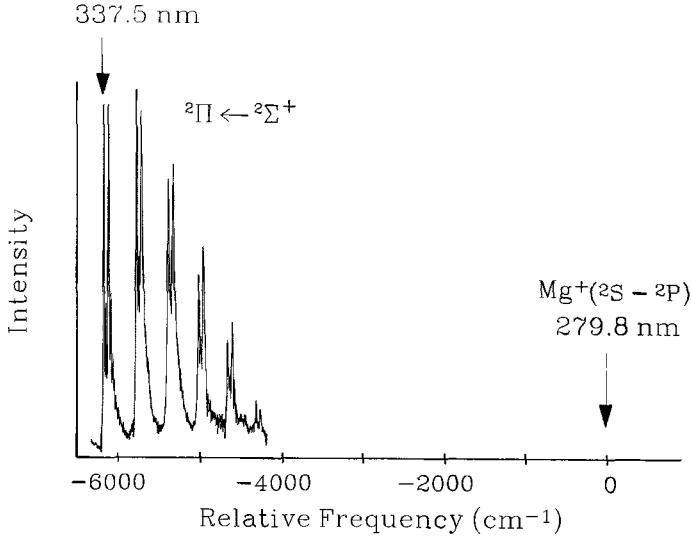

Figure 11. Photodissociation excitation spectrum for Mg^+–CO_2 measured to the red of the $^2P \leftarrow ^2S$ atomic transition. The Mg^+ fragment is detected as the excitation laser is scanned. The progression of doublet bands confirms that the complex is linear, and by analogy to the rare gas complexes the transition is assigned as $^2\Pi \leftarrow ^2\Sigma^+$.

state ($r'_e = 1{\cdot}99$ Å) relative to the ground state ($r''_e = 2{\cdot}10$ Å). We therefore assign this progression to the Mg^+–CO_2 stretching mode. The frequency of 381·8 cm^{-1} which we derive compares to the theoretical prediction of 359 cm^{-1} for this mode in the $^2\Pi$ state [28].

Because the main features in the spectrum are assigned to the metal–ligand stretch progression, we again have access to the dissociation coordinate of the system. Although a proper description of the dissociation of the system should include all the vibrational coordinates, a pseudo-diatomic treatment can be used without introducing significant errors. For this treatment, we treat the complex as if the Mg^+–CO_2 mode were the only one for a diatomic system and fit the excited potential with the Birge–Sponer method described above. The excited state dissociation energy we derive is 11 198 cm^{-1}. As before, we use the known atomic asymptotes and the measured origin energy of the complex spectrum to perform a cycle, yielding the ground state dissociation energy of the complex. The value obtained is 5 154 cm^{-1}, or 14·7 kcal mol^{-1}. This compares favourably with the theoretical prediction of 16·4 kcal mol^{-1} [28]. Owing to the pseudo-diatomic approximation, this value for the dissociation energy underestimates the true value by a factor approximately equivalent to the zero point energy in the bending mode. Although we do not measure this frequency, it should be about 100 cm^{-1}, and the mode is doubly degenerate. This correction would add about 100 cm^{-1}, or 0·3 kcal mol^{-1} to our present value.

The spin–orbit interaction in this linear molecular system is interesting to compare to that seen earlier for the rare gas complexes. While all of the rare gas systems exhibited a $^2\Pi_{1/2,\,3/2}$ doublet with a splitting greater than the expected 61 cm^{-1} value, the CO_2 complex splitting of 56 cm^{-1} is slightly less than this value. This reduction could be caused by partial sharing of Mg^+ (3p) electron density into a CO_2 Rydberg $p\pi$ orbital. Such orbitals would be of the correct symmetry for wavefunction mixing, and the light-atom nature of CO_2 could result in a lowered spin–orbit interaction. However, this effect, if it exists at all, is quite small relative to the increased spin–orbit interaction in the rare gas systems.

Table 4 shows the comparison of the vibrational frequencies, electronic transition energies and dissociation energies measured for the Mg^+–CO_2 complex with the values predicted theoretically by Bauschlicher and coworkers [28]. The agreement between theory and experiment is remarkable on every parameter, especially considering the difficulty encountered by theory in the treatment of excited state problems. Because of this agreement, we conclude that the structure and bonding picture presented by theory for this system must be correct. Mg^+–CO_2 is a linear ion–molecule complex with bonding dominated by the charge–quadrupole interaction. This is the first metal ion–molecular complex to be studied by theory and experiment with this degree of detail so that the structure and bonding could be determined.

6. Mg^+–H_2O complexes

Magnesium ion–water complexes are produced by seeding a small amount of water vapour into an expansion of argon or CO_2, using the conical nozzle. The mono-ligand complex Mg^+–H_2O is predicted by theory [29] to have C_{2v} symmetry with the metal ion bound to the oxygen end of water through the charge–dipole interaction. The electronic state level structure was discussed earlier, and is shown in

Table 4. Electronic state origins, vibrational constants and dissociation energies determined for the Mg^+–CO_2 complex and their comparison to the predictions of theory [19]. All parameters are given in cm^{-1} units except the dissociation energies, which are also given in $kcal\,mol^{-1}$.

Parameter	Experiment			Theory [28]	
	$^2\Pi_{1/2}$	$^2\Pi_{3/2}$	$X^2\Sigma^+$	$^2\Pi$	$X^2\Sigma^+$
Electronic origin	29625	29681	0	30900	0
CO_2 asym. stretch				2630	2613
CO_2 sym. stretch				1522	1502
CO_2 bend				740	752
Mg^+–CO_2 stretch	381·8	385·1		359	250
Mg^+–CO_2 bend				87	84
Dissociation energy (D_0)	11198 (32·0 $kcal\,mol^{-1}$)		5154 (14·7)	10668 (30·5)	5736 (16·4)

figure 7. The bond distance in the ground state is predicted by Bauschlicher and coworkers to be 2·05 Å, and the ground state dissociation energy is calculated to be $31{\cdot}2\,kcal\,mol^{-1}$ [29].

The photodissociation excitation spectra for Mg^+–H_2O and Mg^+–D_2O are shown in figure 12. In both systems, the spectra are recorded in the Mg^+ fragment channel. These spectra begin at an energy of approximately $28\,400\,cm^{-1}$, which is red-shifted by about $7000\,cm^{-1}$ from the atomic Mg^+ transition. Unlike the relatively simple spectra measured for the previous complexes, these spectra have many more bands, the bands have tightly spaced multiplet structure, and there is no simple pattern recognizable at first glance. This immediately suggests that the vibronic patterns arise from activity in more than one vibrational mode, which does indeed turn out to be the case. However, the assignment of the various modes active in this spectrum is a significant undertaking.

The first step in the assignment of this spectrum is the recognition that the closely spaced multiplets associated with the bands arise from partially resolved rotational structure. The observation of rotational structure indicates that at least one rotational constant of the complex is large with respect to our laser bandwidth ($\sim 1\,cm^{-1}$). This is in fact expected if the complex has the planar C_{2v} structure predicted by theory, with Mg^+ bound electrostatically to oxygen on the C_2 symmetry axis. In this structure, the two hydrogen atoms in the water molecule are spaced about the C_2 axis in the same way that they are in the isolated water molecule. The constant for rotation of these atoms in the complex should have about the same value as it does in isolated H_2O, or about $14\,cm^{-1}$. It is therefore not surprising that there would be resolved rotational structure, if the theoretical structure is correct. The analysis of this rotational structure makes it possible to confirm the structure of the complex, as described below. It also makes it possible to assign the vibrational bands to specific vibrational motions, because the patterns in the rotational structure depend on the vibronic symmetry species.

To confirm that the multiplet structure is indeed rotational in origin, we must analyse it in some detail. We begin with the premise that the theoretical structures

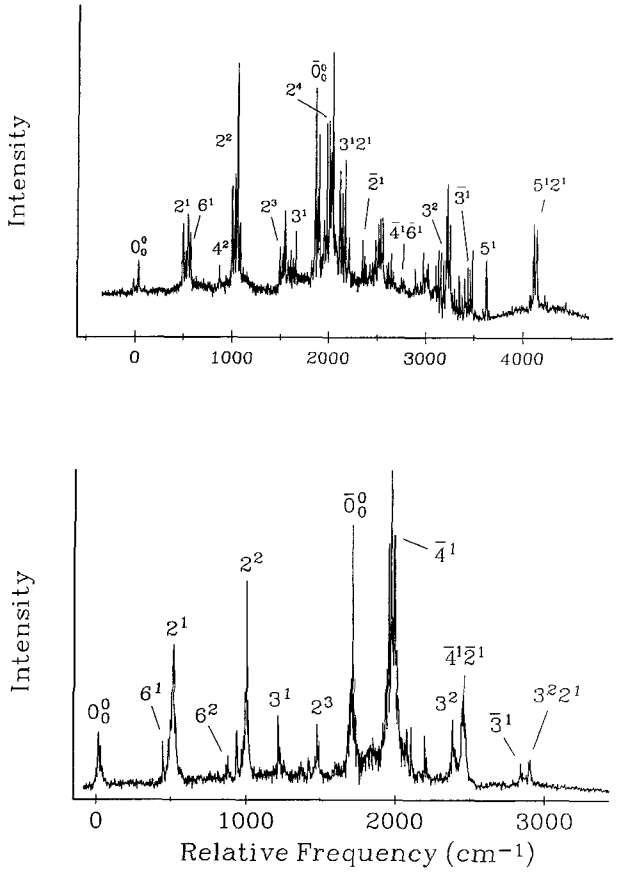

Figure 12. Photodissociation excitation spectra measured for Mg^+–H_2O (top) and Mg^+–D_2O (bottom) complexes. Vibronic activity is measured in several modes which are numbered here and described in the text. Portions of the two electronic transitions $^2B_2 \leftarrow X^2A_1$ and $^2B_1 \leftarrow X^2A_1$ are shown. The multiplet structure of the bands in the Mg^+H_2O spectrum is due to partially resolved rotational structure.

are approximately correct for the ground and excited electronic states of the complex, and we calculate rotational constants from these structures. We obtain the values A, B, $C = 14{\cdot}254$, $0{\cdot}360$ and $0{\cdot}351\,cm^{-1}$ for the ground state, and A, B, $C = 14{\cdot}033$, $0{\cdot}390$ and $0{\cdot}379\,cm^{-1}$ for the lower lying $^2B_2$ excited state. The only significant difference between these two states is that the Mg^+–OH_2 bond distance is contracted in the excited state. These rotational constants indicate that the complex is an asymmetric top in both states, but that it is vanishingly close to a prolate symmetric top. For example, the assymmetry parameter calculated is $-0{\cdot}9987$ for the ground state. Since the system is so close to symmetric, and since our spectra have only moderate resolution, we expect that the main features observed will be consistent with those for a symmetric top system. In a symmetric top system, the rotational structure observed in a vibrational band of an electronic transition can be either *parallel*-type or *perpendicular*-type, depending on the vibronic symmetry of the band. We must therefore consider the vibrational symmetry species of the modes for

this molecule. Although we have not yet assigned the vibrational modes, the first band in the spectrum is likely to be an electronic origin because it has no isotopic shift. Studies of the spectra under various conditions produce no evidence for vibrational hot-bands. Therefore, we tentatively assign the first band to the origin of the expected $^2B_2 \leftarrow ^2A_1$ transition. This pure electronic transition is allowed by virtue of the b_2 (y) component of the dipole matrix element, and therefore a perpendicular-type band is expected for the rotational structure (selection rules: $\Delta J = \pm 1,0$; $\Delta K = \pm 1$). A perpendicular band structure would also be expected for the origin of an excited state with $^2B_1$ symmetry.

The appearance of a perpendicular band for a symmetric top has a very characteristic pattern dominated by ^PQ and ^RQ sub-band branches, whose positions are deterimined primarily by the value of the A rotational constant. Additionally, the presence of two indistinguishable hydrogen atoms causes a 3:1 intensity alternation for K even : odd lines due to the nuclear spin statistical weighting factors. We have therefore measured the profile of this origin band on an expanded scale, which is shown in figure 13. We have also calculated a simulated spectrum using the parameters and rules described here to see if it is consistent with the measured one. The rotational temperature used in this simulation is 10 K, and the rotational constants have been adjusted slightly from the initial estimates provided by the theoretical structure (A'', $B'' = 13{\cdot}521$, $0{\cdot}364\ cm^{-1}$; A', $B' = 13{\cdot}521$, $0{\cdot}375\ cm^{-1}$). As shown in the two frames of figure 13, the simulated spectrum is in good agreement with the measured one. This agreement is significant because of the limited number of adjustable parameters in the simulation and the restrictive rules in line intensities. Due to the unresolved structure present, the fit is not completely unique. For example, a small change in the B rotational constant could be compensated for by a small variation in temperature. However, if the temperature in the simulation exceeds about 15 K, additional side branches which are not observed appear in the simulation. From the agreement seen here, we conclude that the molecule must have a planar C_{2v} structure in approximately the structure suggested by theory. Otherwise, the nuclear spin alternation in line intensities would not be observed.

To further test this structure, we have also measured and simulated the lowest energy origin band for Mg^+–D_2O [20]. In this system, the rotational constant for hydrogen atom motion should be reduced by exactly a factor of two, and the nuclear spin intensity alternation changes to a factor of 2:1 for K even : odd. This latter change occurs because the hydrogen atoms are *fermions* while the deuterium atoms are *bosons*, and the selection rules and statistical weights change for these two systems. Again, without making any changes in the structural parameters of the complex or its temperature, we obtain a good match between the simulated and measured spectra. Therefore, we conclude that the qualitative features of the theoretical structure are correct. Mg^+–H_2O is a planar molecule with C_{2v} symmetry and the water molecule has nearly the same structure as isolated H_2O. No other structure could produce a match with the simulated and measured rotational profiles for both isotopic species.

With the understanding of the rotational structure, it is also possible to obtain a convincing assignment for all of the vibrational bands in the spectrum, and to identify the presence of a second electronic state in the spectrum. The second electronic state is identified by its isotope shift between the Mg^+–H_2O and Mg^+–D_2O spectra, and by its different rotational band profiles. It is observed at an energy $1869\ cm^{-1}$ above the first origin and the origin band has a perpendicular

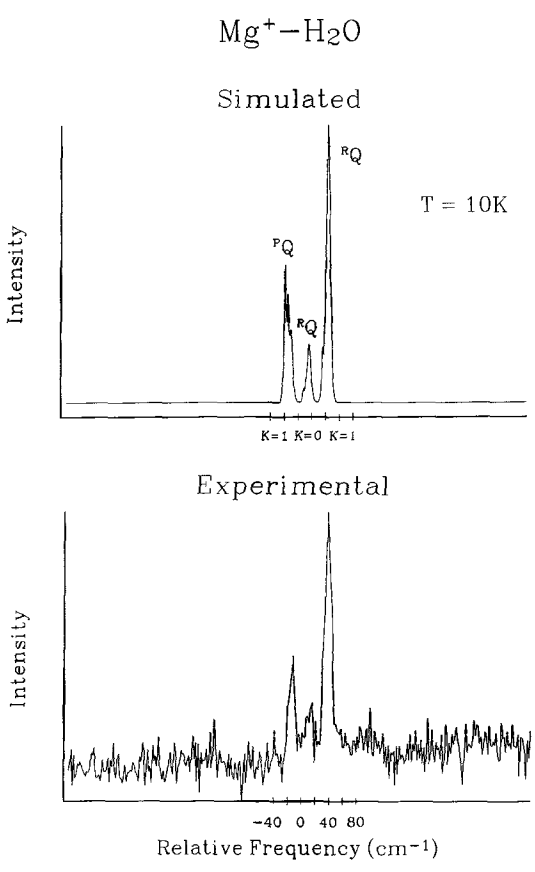

Figure 13. An expanded view of the origin band of the $^2B_2 \leftarrow X^2A_1$ transition for Mg^+-H_2O and a simulation of this band assuming that it is a perpendicular-type band for a prolate symmetric top. The rotational constants used for the simulation are $A' = 13{\cdot}521$, $B' = 0{\cdot}375$, $A'' = 13{\cdot}521$, $B'' = 0{\cdot}364\,cm^{-1}$, and the rotational temperature is 10 K.

band profile with a smaller spacing between the sub-band branches. In keeping with the theoretical predictions for this state, we assign it to the $^2B_1 \leftarrow ^2A_1$ transition.

The C_{2v} molecular structure of this complex gives rise to six vibrational modes. These are respectively, the H_2O symmetric stretch (ν_1, a_1 symmetry), the metal–ligand symmetric stretch (ν_2, a_1 symmetry), the H_2O scissors motion (ν_3, a_1 symmetry), the Mg^+-H_2O out-of-plane bend (ν_4, b_1 symmetry), the H_2O asymmetric stretch (ν_5, b_2 symmetry) and the Mg^+-H_2O in-plane bend (ν_6, b_2 symmetry). Assuming again that the lower level is $v = 0$ in the $^2A_1$ ground state, transitions to all of the a_1 modes in the $^2B_2$ electronic state are vibronically allowed, and they should have perpendicular-type rotational profiles. On the other hand, transitions to b_2 modes are vibronically allowed, but the bands have parallel-type rotational profiles. At the low temperatures here, parallel-type profiles have essentially a single peak, rather than the triplet structure shown in figure 13 for the perpendicular bands. In the upper $^2B_1$ state, a_1 and b_1 modes are vibronically allowed. The a_1 bands have perpendicular-type profiles and the b_1 bands have parallel-type profiles. With this

information, the knowledge that the water molecule and its known vibrational frequencies are only slightly perturbed by the electrostatic bond, and the predicted frequencies for the metal–ligand bending and stretching modes, essentially all the vibrational modes in the two electronic states can be assigned for both the H_2O and D_2O complexes. The details of these assignments are discussed in our earlier papers [20]. These assignments are given in table 5. A final aspect of this analysis is that the overall assignment of the vibrational modes is only possible if the lower of the two excited electronic states is assigned as $^2B_2$ and the upper state is assigned as $^2B_1$, as predicted by theory.

As indicated in the vibrational band assignments in figure 12, we observe the origin and four additional members of a progression in the Mg^+–H_2O stretching mode. As we have discussed earlier for the other complexes, this mode is the dissociation coordinate of the molecule. Again, assuming pseudo-diatomic behaviour, and neglecting the other modes of the system, we can derive a dissociation energy for the excited state of the system and we can perform the cycle indicated earlier to obtain the ground state dissociation energy. The excited $^2B_2$ state of Mg^+–H_2O has a dissociation energy of 15 787 cm^{-1}, and the ground state has a dissociation energy of 8 514 cm^{-1}. This latter value corresponds to 24·3 kcal mol^{-1}. Table 5 presents a summary of the spectroscopic constants for the magnesium–water complexes, including these dissociation energies, and their comparison to the predictions of the theoretical calculations of Bauschlicher and coworkers. Armentrout *et al.* have recently studied the collision induced dissociation of Mg^+–H_2O,

Table 5. Electronic state origins, vibrational constants and dissociation energies determined for the Mg^+–H_2O complex and their comparison to the predictions of theory [20]. All units are cm^{-1} except that the dissociation energies are also given in kcal mol^{-1}. Mg^+–H_2O and Mg^+–D_2O stretching constants ($^2B_2$ state) are ω_e values, while other values are fundamental frequencies ($\Delta G_{1/2}$). Vibrational constants for Mg^+–D_2O are given in parentheses.

	Experiment			Theory*		
Parameter	$^2B_2$	$^2B_1$	X^2A_1	$^2B_2$	$^2B_1$	X^2A_1
Electronic origin	28 396	30 267	0	27 849	29 797	0
H_2O stretch	518·0	489		505	471	394
	(502·9)	(468)		(489)		
Mg^+H_2O in-plane wag	567	561		672	651	579
	(431)			(502)		
Mg^+–H_2O out-of-plane wag	417	332		496	300	460
		(281)		(380)		(425)
H_2O bend	1614	1577		1659		1659
	(1199)	(1130)		(1229)		(1227)
H_2O asym. stretch	3632			3637		3622
				(2693)		(2692)
H_2O sym. stretch	3360			3574		3557
				(2607)		(2595)
Dissociation energy (D_0)	15 787		8 514	17 068	15 599	10 912
	(45·1 kcal mol^{-1})		(24·3)	(48·8)	(44·6)	(31·2)

and they obtain a dissociation energy of 28·4 kcal/mol [50] which is slightly higher than our value. The difference between these values may be caused by our approximation of a Morse potential form for this system. We have also used the pseudo-diatomic approximation described earlier for this system, since the bending mode frequencies in the ground state have not been measured. We estimate that because of this approximation, a factor of 1·5 kcal mol^{-1} should be added to our present value.

As shown in table 5, there is an overall very good agreement between our experimental data for magnesium–water complexes and the theoretical predictions for this system. Our spectroscopic constants should be regarded as much more accurate than the theory, but theory does predict the correct order of excited states and their relative positions quite well. Our dissociation energies are subject to greater errors, but judging by the recent Armentrout data, we are within about 10% of the correct value. When viewed as a whole, the experimental results agree so well with the various predictions of theory that we must again conclude that theory has predicted the correct structure and bonding for this system. Mg^+–H_2O is an electrostatic complex, bound by charge–dipole forces, with a planar C_{2v} structure and the water molecule is only slightly perturbed by this interaction.

7. Mg^+–N_2 complexes

Mg^+–N_2 is one of the most interesting systems we have studied to date because of the difficulties encountered by theory in describing this system. Maitre and Bauschlicher [51] investigated this system after their various successes with the other systems described above. Based on this experience, they initially treated this system at low levels of theory (Möller–Plesset MP-2 perturbation theory), which had been sufficient to describe the CO_2 and water complexes in their ground and excited states. At this level of theory, the nitrogen complex is predicted to be linear in its ground and excited states and to be weakly bound by charge–quadrupole forces. The binding energy in the ground state is calculated to be $D_0 = 4{\cdot}1$ kcal mol^{-1}. The excited states for this kind of linear system are expected to follow the pattern of levels shown in figure 6. The excited $^2\Pi$ state is calculated to be bound by 24·6 kcal mol^{-1} and to have a metal–ligand stretching mode frequency of 384 cm^{-1}. Thus, we expected the electronic spectroscopy of this system to be very similar to that of Mg^+–CO_2, with about the same excited state vibrational frequency, vibrational bands doubled by a spin-orbit splitting near 60 cm^{-1}, and a slighty greater red shift in the $^2\Pi \leftarrow {}^2\Sigma^+$ spectrum (origin predicted at 27 274 cm^{-1}). As it turned out, these expectations were not correct.

The photodissociation spectrum measured for Mg^+–N_2 is shown in figure 14. Figure 14 shows only the low energy region of a system that extends to higher energy and becomes progressively more congested. The spectrum shown consists of a series of sharp vibrational bands, but the patterns found are not what we expected based on the theory for this system. The vibrational bands do not seem to have the simple doublet structure expected for a linear $^2\Pi$ state, and the bands observed cannot be assigned to a single metal–ligand stretch progression that would also be expected. There is also no evidence for a progression in a frequency near 384 cm^{-1}. Instead, the bands observed can be assigned to a progression in a frequency of $\omega_e' = 1137$ cm^{-1}, with a combination band accompanying each progression member having a frequency ($\Delta G_{1/2}$) of about 480 cm^{-1}. The 1137-cm^{-1} progression extends from its first member observed near 25 000 cm^{-1} to beyond 30 000 cm^{-1}. It shows a

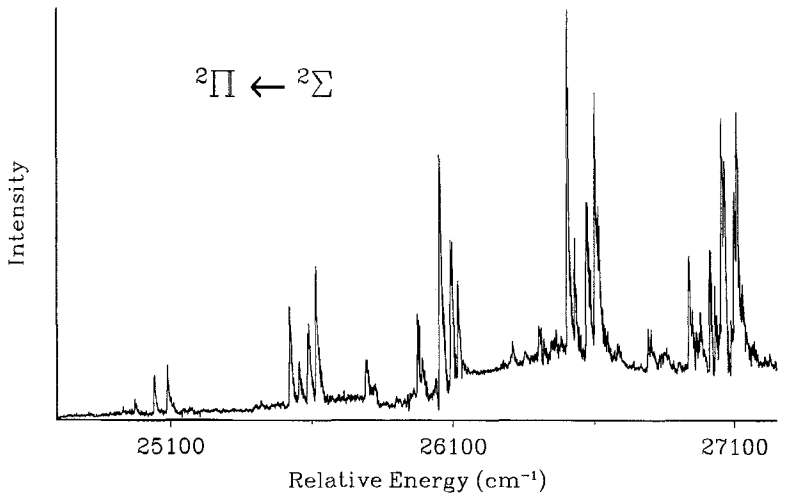

Figure 14. Photodissociation excitation spectrum of Mg^+–N_2.

magnesium isotope effect consistent with this mode being a Mg^+–L stretch, with the first band observed assigned as $v=2\leftarrow v''=0$, yielding an extrapolated origin for the system at 22 882 cm^{-1}. These various spectroscopic observations are not consistent with the weakly bound system predicted by the theory. Therefore, Maitre and Bauschlicher examined the system at higher levels of theory.

At correlated levels of theory (configuration interaction based on an averaged complete active space-self-consistent field (CAS-SCF) wavefunction) the theory reveals a possible explanation for the interesting spectrum we have observed. The excited state minimum no longer occurs in the linear configuration, while the ground state remains linear. Actually, theory indicates that the excited state attributed before to the $^2\Pi$ state now has *two* minima, one with C_{2v} symmetry (the $^2B_2$ state) and one in the linear configuration ($^2\Pi$). The $^2B_2$ state lies lower in energy by 1761 cm^{-1}, and corresponds to an 'inserted' bonding arrangement. It is separated from the linear $^2\Pi$ state by a transition state in the C_s configuration, and a barrier height of about 5000 cm^{-1}. It is not clear which of the excited potentials we probe with our spectroscopy. The Franck–Condon factors should be most favourable to access the excited $^2\Pi$ state, because it has the same linear configuration as the ground state. However, this state should have a spin–orbit splitting near 60 cm^{-1}. The main progression members appear to be doublets with spacings of about 40 cm^{-1}, so this is a possible assignment if we assume a low value for the spin–orbit interaction. The combination bands which appear at approximately 480 cm^{-1} above each of the main progression members are split into additional multiplets, perhaps by vibronic interaction involving the bending mode. It is difficult to confirm these possibilities, however, because the excited state vibrational frequencies have not yet been obtained at the higher level of theory. The interpretation of this spectrum is therefore still under active investigation.

8. Other magnesium ion complexes

Over the last few years we have attempted photodissociation spectroscopy experiments like those described here on several other magnesium ion complexes for

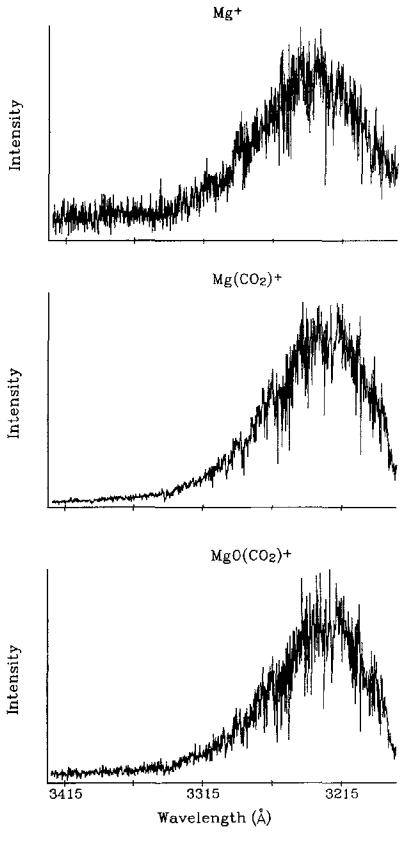

Figure 15. Photodissociation excitation spectrum of Mg^+–$(CO_2)_2$. The spectrum is broad with no vibrational structure in any of the three product channels observed.

which we were not able to obtain sharp spectra. Some of these systems include Mg^+–O_2, Mg^+–benzene, Mg^+–methanol and Mg^+–N_2O. In these systems, the photodissociation spectra are continuous, with no resolved vibrational structure. Additionally, fragment channels other than the Mg^+ ion are often observed, indicating that there is photoinduced chemistry in the complexes. A more extensive discussion of these photochemical systems is presented elsewhere [48]. However, a brief mention of some of these systems is included here for comparison to the systems described above.

The first evidence for photo-induced chemistry in these complexes was found for the Mg^+–CO_2 system. In this complex, the spectrum in the region assigned to the $^2\Sigma^+ \leftarrow ^2\Sigma^+$ transition is a continuum, and both the Mg^+ and MgO^+ product channels exhibit the same spectrum. The metal oxide channel is attributed to a state-specific reaction occurring in the excited state of the complex after photoexcitation [49]. Similar metal oxide channels and continuous spectra are observed for Mg^+–O_2, which theory predicts to have the Mg^{2+}–O_2^- ion-pair structure, for Mg^+–methanol and for Mg^+–N_2O. Additionally, we have also tried to measure spectra for several multi-ligand complexes without much success. Mg^+–$(CO_2)_2$ is predicted to have a C_{2v} structure [19]. Figure 15 shows the excitation spectrum for this complex in the 340 nm region near the predicted $^2B_1 \leftarrow ^2A_1$ electronic transition. As indicated, there

are three fragment channels, Mg^+, Mg^+–CO_2 and MgO^+–CO_2. Each of these fragment channels has the same wavelength dependence, indicating an electronic transition with no resolved vibrational structure. We presume that a reaction occurs within the complex so fast that the excited state is lifetime broadened, but no direct measurements of the lifetimes are yet available. The only other multi-CO_2 complex studied thus far is Mg^+–$(CO_2)_6$, which also has a continuous spectrum in several fragment channels. Similar problems have arisen when we have attempted to measure spectra for multi-ligand complexes of magnesium ion with water or argon.

Perhaps the most interesting example of photochemical dynamics occurs for complexes of magnesium ion with benzene. In this system, the lowest electronic transition is no longer the solvated $^2P \leftarrow ^2S$ atomic system. Instead, it is a *charge transfer* transition [16]. This arises because there is only a small difference between the ionization potentials of magnesium atom ($IP = 7{\cdot}646\,eV$) and the benzene molecule ($IP = 9{\cdot}24\,eV$). In the Mg^+–benzene complex, which is bound by charge-induced dipole forces, the positive charge is localized on the magnesium atom because it has the lower ionization potential. However, when energy in excess of about $1{\cdot}59\,eV$ is provided to the complex by photoexcitation, the charge can be transferred to the benzene moiety. This is possible at wavelengths to the blue of about 778 nm. If enough additional energy is provided to dissociate the complex, the benzene fragment ion may be produced. Experimentally, we observe a continuous spectrum in the $C_6H_6^+$ channel with an onset at 450 nm [16]. While this continuous spectrum does not provide detailed information on the structure and vibrational frequencies of the complex, it does afford a method of determining the approximate dissociation energy. As noted above, the energy required to produce the benzene cation channel must exceed the combined ionization potential difference (ΔIP) and the dissociation energy of the complex (D_0''). Therefore, the measurement of the onset of this channel ($h\nu_{CT}$) followed by the subtraction of the IP difference produces an upper limit for the dissociation energy,

$$D_0'' \leqslant h\nu_{CT} - \Delta IP.$$

Although this procedure is only guaranteed to provide an upper limit to the dissociation energy, it often provides a value in close agreement with dissociation energies measured by other techniques [16]. For Mg^+–benzene, we obtain a value of $26{\cdot}9\,kcal\,mol^{-1}$, while the theoretical value for this dissociation energy is $30{\cdot}4\,kcal\,mol^{-1}$ [16]. The charge transfer channel is observed for many metal-ion complexes with benzene because of the low ionization potential of benzene. This channel is also observed for Mg^+–acetone. For the small molecule complexes discussed earlier in this review, the ligand IP is high enough so that charge transfer resonances would be found in the deep ultraviolet of vacuum ultraviolet regions of the spectrum, beyond the wavelengths yet studied for these systems.

9. Conclusions

We have described here a summary of several studies of the spectroscopy of magnesium ion–molecular complexes using mass-selected photodissociation. These studies represent a significant fraction of all of the existing spectroscopy on metal-ion complexes. We find that laser vapourization techniques can be used to produce a number of ion–molecule complexes which are weakly bound by various forms of electrostatic forces. In some systems, sharp spectra can be obtained which make it possible to unravel the details of structures and bonding. In other systems, excited state photochemical channels work to obscure the sharp structure of spectra, but

Table 6. A comparison of the metal–ligand vibrational frequencies (excited state) and dissociation energies of several magnesium ion complexes.

	Mg^+–L Stretch (cm^{-1})		D_0'' ($kcal\,mol^{-1}$)		
Complex	Exp.	Theory [26–33]	Exp.	Theory [26–33]	Structure
Mg^+–Ar	272	–	3·37	3·25	Diatomic
Mg^+–Kr	258	–	5·2	–	Diatomic
Mg^+–Xe	258	–	11·7	–	Diatomic
Mg^+–CO_2	382	359	14·7	16·4	Linear
Mg^+–H_2O	517	505	25·0	32·2	C_{2v}
Mg^+–N_2	1137		3·03	4·1	Linear
Mg^+–benzene			26·9	30·4	

fascinating photochemical dynamics are revealed. In systems where comparisons are possible, the structure and bonding measured for these metal complexes are in remarkably good agreement with theory. This agreement indicates that theory is well suited for these problems, especially when light metals and small molecules are chosen for study. Table 6 presents an overall comparison of the metal–ligand stretching mode frequencies observed for the different complexes and their dissociation energies. The trends in the dissociation energies are particularly satisfying and completely consistent with the concepts of electrostatic bonding. The charge-induced dipole systems exhibit the weakest binding (except for the most polarizable xenon system), the charge–quadrupole system Mg^+–N_2 has about the same binding as Mg^+–Ar, consistent with the small quadrupole moment and small polarizability of N_2. The charge–quadrupole and charge–dipole systems Mg^+–CO_2 and Mg^+–H_2O are significantly more strongly bound than all the other systems except for Mg^+–benzene, whose binding is enhanced by the large polarizability of benzene.

Further spectroscopic studies are presently underway to extend these studies in new directions. For example, the spectra accumulated so far were done under moderate laser resolution. New lasers systems in our lab will make it possible to use higher resolution to measure rotationally resolved spectra. Such spectra can reveal more detail about the structures of these complexes, particularly their bond distances. We are also extending the studies to other metal ions and other ligands. We are particularly interested in metal *pi* complexes, and plan studies on systems such as M^+–ethylene and M^+–acetylene. To address the difficulties with excited state photochemistry, we have adapted the new technique of *mass analysed threshold ionization* (MATI) spectroscopy to the study of metal complexes [22]. This technique is a form of high-resolution photoelectron spectroscopy which can be used to probe directly the ground electronic state of these cation complexes. Through the application of new techniques and the continued interaction with our theoretical colleagues, we expect new studies of metal ion complexes to continue to reveal fundamental details of metal chemistry and metal-ligand bonding.

Acknowlegments

This research is funded by the Air Force Office of Scientific Research (grant AFOSR-91-0001) through the high Energy Density Materials (HEDM) program and by the National Science Foundation through grants CHE-90082246 and CHE-9307907. We appreciate helpful discussions with Charlie Bauschlicher and with Bill Breckenridge.

References

[1] KEBARLE, P., 1977, *Ann. Rev. Phys. Chem.*, **28,** 445.

[2] (*a*) CASTLEMAN, A. W., HOLLAND, P. M., LINDSAY D. M., and PETERSON, K. I., 1978 *J. Am. Chem. Soc.*, **100,** 6039; (*b*) CASTLEMAN, A. W., 1978, *Chem. Phys. Lett.*, **53,** 560; (*c*) HOLLAND, P. W., and CASTLEMAN, A. W., *J. chem. Phys.*, **76,** 4195; (*d*) GLEIN, K. L., GUO, B. C., KEESEE, R. G., and CASTLEMAN, A. W., 1989, *J. phys. Chem.*, **93,** 6805; (*e*) GUO, B. C., PURNELL, J. W., and CASTLEMAN, A. W., 1990, *Chem. Phys. Lett.*, **168,** 155; (*f*) GUO, B. C., and CASTLEMAN, A. W., 1991, *Ibid.*, **181,** 16.

[3] MAGNERA, T. F., DAVID, D. E., and MICHL, J., *Ibid.*, *J. Am. Chem. Soc.*, **111,** 4100.

[4] MARINELLI, P. J., and SQUIRES, P. R., 1989, *J. Am. Chem. Soc.*, **11,** 4101.

[5] BOUCHARD, F., HEPBURN, J. W., and MCMAHON, T. B., 1989, *J. Am. Chem. Soc.*, **111,** 8934.

[6] (*a*) SCHULTZ, R. H., and ARMENTROUT, P. B., 1993, *J. phys. Chem.*, **97,** 596; (*b*) CHEN, Y. M., and ARMENTROUT, P. B., 1993, *Chem. Phys. Lett.*, **210,** 123.

[7] (*a*) HETTICH, R. L., and FREISER, B. S., 1987, *J. Am. Chem. Soc.*, **109,** 3543; (*b*) FREISER, B. S., 1989, *Chemtracts-Anal. and Phys. Chem.*, **1,** 65; (*c*) LECH, L. M., 1988, Ph. D. Thesis, Purdue University; (*d*) HETTICH, R. L., JACKSON, T. C., STANKO, E. M., and FREISER, B. S., 1986, *J. Am. Chem. Soc.*, **108,** 5086; (*e*) OPERTI, L., TEWS, E. C., and FREISER, B. S., 1988, *Ibid.*, **110,** 3847; (*f*) OPERTI, L., TEWS, E. C., MACMAHON, T. J., and FREISER, B. S., 1989, *Ibid.*, **111,** 9152.

[8] HIGASHIDE, H., KAYA, T., KOBAYASHI, M., SHINCHARA, H., and SATO, H., 1990, *Chem. Phys. Lett.*, **171,** 297.

[9] (*a*) LIU, W. L., and LISY, J. M., 1988, *J. chem. Phys.*, **89,** 605; (*b*) SELEGUE, T. S., MEO, N., DRAVES, J. A., and LISY, J. M., 1992, *Ibid.*, **96,** 7268; (*c*) SELEGUE, T., and LISY, J. M., 1992, *J. phys. Chem.*, **96,** 4143.

[10] (*a*) KEMPER, P. R., HSU, M. T., and BOWERS, M. T., 1991, *J. phys. Chem.*, **95,** 10,600; (*b*) KEMPER, P. R., BUSHNELL, J., VON HELDEN, G., and BOWERS, M. T., 1993, *Ibid.*, **97,** 52.

[11] EL-SHALL, M. S., SCHRIVER, K. E., WHETTEN, R. L., and MAUTNER, M. J., 1989, *J. phys. Chem.*, **93,** 7969.

[12] BLADES, A. T., JAYAWEERA, P., IKONOMOU, M. G., and KEBARLE, P., 1992, *J. chem. Phys.*, **92,** 5900.

[13] HE, K. X., HAMMOND, T. D., WINSTEAD, C. B., GOLE, J. L., and DIXON, D. A., 1991, *J. chem. Phys.*, **95,** 7183.

[14] (*a*) KEMPER, P. R., and BOWERS, M. T., 1991, *J. phys. Chem.*, **95,** 5134; (*b*) VON HELDEN, G., KEMPER, P. R., HSU, M. T., and BOWERS, M. T., 1992, *J. chem. Phys.*, **96,** 6591.

[15] (*a*) SHEN, M. H., and FARRAR, J. M., 1989, *J. phys. Chem.*, **93,** 4386; (*b*) SHEN, M. H., and FARRAR, J. M., 1991, *J. chem. Phys.*, **94,** 3322.

[16] (*a*) WILLEY, K. F., CHENG, P. Y., TAYLOR, T. G., BISHOP, M. B., and DUNCAN, M. A., 1990, *J. phys. Chem.*, **94,** 1544; (*b*) WILLEY, K. F., CHENG, P. Y., BISHOP, M. B., and DUNCAN, M. A., 1991, *J. Am. Chem. Soc.*, **113,** 4721; (*c*) WILLEY, K. F., YEH, C. S., ROBBINS, D. L., and DUNCAN, M. A., 1992, *J. phys. Chem.*, **96,** 9106.

[17] (*a*) LESSEN, D. E., and BRUCAT, P. J., 1989, *J. chem. Phys.*, **90,** 6296; (*b*) LESSEN, D. E., and BRUCAT, P. J., 1989, *Ibid.*, **91,** 4522; (*c*) LESSEN, D. E., ASHER, R. L., and BRUCAT, P. J., 1993, *Advances in Metal and Semiconductor Clusters*, edited by M. A., Duncan, (Greenwich, CT: JAI Press), Vol. I, p. 267.

[18] (*a*) LESSEN, D. E., ASHER, R. L., and BRUCAT, P. J., 1990, *J. chem. Phys.*, **93,** 6102; (*b*) LESSEN, D. E., ASHER, R. L., and BRUCAT, P. J., 1991, **95,** 1414.

[19] (*a*) WILLEY, K. F., YEH, C. S., ROBBINS, D. L., and DUNCAN, M. A., 1992, *Chem. Phys. Lett.*, **192,** 179; (*b*) YEH, C. S., WILLEY, K. F., ROBBINS, D. L., PILGRIM, J. S., and DUNCAN, M. A., 1993, *J. Chem. Phys.*, **98,** 1867.

[20] (*a*) YEH, C. S., WILLEY K. F., ROBBINS, D. L., PILGRIM, J. S., and DUNCAN, M. A., 1992, *Chem. Phys. Lett.*, **196,** 233; (*b*) WILLEY, K. F., YEH, C. S., ROBBINS, D. L., PILGRIM, J. S., and DUNCAN, M. A., 1992, *J. chem. Phys.*, **97,** 8886.

[21] PILGRIM, J. S., YEH, C. S., and DUNCAN, M. A., 1993, *Chem. Phys. Lett.*, **210,** 322.

[22] WILLEY, K. F., YEH, C. S., and DUNCAN, M. A., 1993, *Chem. Phys. Lett.*, **211,** 156.

[23] MISAIZU, F., SANEKATA, M., TSUKAMOTO, K., FUKE, K., and IWATA, S., *J. phys. Chem.*, **96,** 8259.

[24] PILGRIM, J. S., YEH, C. S., BERRY, K. R., and DUNCAN, M. A., 1994, *J. chem. Phys.*, **100,** 7945.

[25] DING, L. N., YOUNG, M. A., KLEIBER, P. D., STWALLEY, W. C., and LYYRA, A. M., 1993, *J. phys. Chem.*, **97,** 2181.
[26] (*a*) BAUSCHLICHER, C. W., and PARTRIDGE, H., 1991, *J. phys. Chem.*, **95,** 3946; (*b*) BAUSCHLICHER, C. W., and PARTRIDGE, H., 1991, *Chem. Phys. Lett.*, **181,** 129; (*c*) SODUPE, M., BAUSCHLICHER, C. W., LANGHOFF, S. R., and PARTRIDGE H., 1992, *J. phys. Chem.*, **96,** 2118; (*d*) BAUSCHLICHER, C. W., SODUPE, M., and PARTRIDGE, H., 1992, *J. chem. Phys.*, **96,** 4453; (*e*) PARTRIDGE, H., BAUSCHLICHER, C. W., and LANGHOFF, S. R., 1992, *J. phys. Chem.*, **96,** 5350; (*f*) BAUSCHLICHER, C. W., 1994, private communication.
[27] (*a*) BAUSCHLICHER, C. W., PARTRIDGE, JR., H., and LANGHOFF, S. R., 1989, *J. chem. Phys.*, **91,** 4733; (*b*) BAUSCHLICHER, C. W., PARTRIDGE, JR., H., and LANGHOFF, S. R., 1990, *Chem. Phys. Lett.*, **165,** 272; (*c*) PARTRIDGE, H., BAUSCHLICHER C. W., JR., and LANGHOFF, S. R., 1992, *J. phys. Chem.*, **96,** 5350.
[28] SODUPE, M., BAUSCHLICHER, C. W., and PARTRIDGE, H., 1992, *Chem. Phys. Lett.*, **192,** 185.
[29] SODUPE, M., and BAUSCHLICHER, C. W., 1992, *Chem. Phys. Lett.*, **195,** 494.
[30] BAUSCHLICHER, C. W., 1993, *Chem. Phys. Lett.*, **201,** 11.
[31] SODUPE, M., and BAUSCHLICHER, C. W., 1993, *Chem. Phys. Lett.*, **203,** 215.
[32] BAUSCHLICHER, C. W., and SODUPE, M., 1993, *Chem. Phys. Lett.*, **214,** 489.
[33] BAUSCHLICHER, C. W., 1994, private communication.
[34] MOORE, C. E., 1971, *Atomic Energy Levels*, National Standard Reference Data Series, National Bureau of Standards, Vol. 35.
[35] FRANKLIN, J. L., DILLARD, J. G., ROSENSTOCK, H. M., HERRON, J. T., DRAXEL, K., and FIELD, F. H., 1969, *Ionization Potentials, Appearance Potentials, and Heats of Formation of Gaseous Positive Ions*, National Standard Reference Data Series, National Bureau of Standards, Vol. 26.
[36] (*a*) DIETZ, T. G., DUNCAN, M. A., POWERS, and SMALLEY, R. E., 1981, *J. chem. Phys.*, **74,** 6511. (*b*) HOPKINS, J. B., LANGRIDGE-SMITH, P. R. R., MORSE, M. D., and SMALLEY, R. E., 1983, *Ibid.*, **78,** 1627.
[37] O'BRIEN, S. C., LIU, Y., ZHANG, Q., HEATH, J. R., TITTEL, F. K., CURL, R. F., and SMALLEY, R. E., 1986, *J. chem. Phys.*, **84,** 4074.
[38] (*a*) LAIHING, K., CHENG, P. Y., TAYLOR, T. G., WILLEY, K. F., PESCHKE, M., and DUNCAN, M. A., 1989, *Analyt. Chem.*, **61,** 1458; (*b*) CORNETT, D. S., PESCHKE, M., LAIHING, K., CHENG, P. Y., WILLEY, K. F., and DUNCAN, M. A., 1992, *Rev. Scient. Instrum.*, **63,** 2177.
[39] LEFEBVRE-BRION, H., and FIELD, R. W., 1986, *Perturbations in the Spectra of Diatomic Molecules*, (Orlando: Academic).
[40] RIGBY, M., SMITH, E. B., WAKEMAN, W. A., and MAITLAND, G. C., 1986, '*The Forces Between Molecules*,' (Oxford: Clarendon Press).
[41] STEINFELD, J. I., 1985, *Molecules and Radiation: An Introduction to Modern Molecular Spectroscopy* (Cambridge, MA: MIT), p. 153.
[42] (*a*) LEROY, R. J., and BERNSTEIN, R. B., 1970, *J. chem. Phys.*, **52,** 3869; (*b*) LEROY, R. J., and BERSTEIN, R. B., 1971, *J. molec. Spectrsc.*, **37,** 109.
[43] BRECKENRIDGE, W. H., JOUVET, C., and SOEP, B., 1994, *Advances in Metal and Semiconductor Clusters*, edited by M. A. Duncan, (Greenwich, CT: JAI Press) Vol. III, in press.
[44] (*a*) SMALLEY, R. E., AUERBACH, D. A., FITCH, P. S. H., LEVY, D. H., and WHARTON, L., 1977, *J. chem. Phys.*, **66,** 3778; (*b*) TELLINGHUISEN, J., RAGONE, A., KIM M. S., AUERBACH, D. J., SMALLEY, R. E., WHARTON, L., and LEVY, D. H., 1979, *Ibid.*, **71,** 1283.
[45] COOPER, D. L., 1981, *J. chem. Phys.*, **75,** 4157.
[46] BRUHL, R., KAPETANAKIS, J., and ZIMMERMAN, D., 1991, *J. chem. Phys.*, **94,** 5865.
[47] BAUMAN, P., ZIMMERMAN, D., and BRUHL, R., 1992, *J. molec. Spectrosc.*, **155,** 277.
[48] YEH, C. S., WILLEY, K. F., ROBBINS, D. L., and DUNCAN, M. A., 1994, *Intl. J. Mass Spectrom. Ion Processes*, **131,** 307.
[49] YEH, C. S., WILLEY, K. F., ROBBINS, D. L., and DUNCAN, M. A., 1992, *J. phys. Chem.*, **96,** 7833.
[50] DALLESKA, N. F., TJELTA, B. L., and ARMENTROUT, 1994, *J. phys. Chem.*, **98,** 4191.
[51] MAITRE, P., and BAUSCHLICHER, C. W., 1994, *Chem. Phys. Lett.*, in press.